REPORT NO. 63

COMPARATIVE STUDY OF TIP CLEARANCE EFFECTS IN COMPRESSORS AND TURBINES

EIJI YOKOYAMA

May 1961

GAS TURBINE LABORATORY
MASSACHUSETTS INSTITUTE OF TECHNOLOGY
CAMBRIDGE · 39 · MASSACHUSETTS

COMPARATIVE STUDY OF TIP CLEARANCE EFFECTS IN COMPRESSORS AND TURBINES

by

EIJI YOKOYAMA

Under the Sponsorship of

General Electric Company
Westinghouse Electric Company

Gas Turbine Laboratory

Report Number 63

Massachusetts Institute of Technology

May 1961

TABLE OF CONTENTS

ACKNOWLEDGEMENT

The author wishes to express his sincere thanks to Professor E. S. Taylor, Director of the Gas Turbine Laboratory, thesis supervisor, for his generous help and many suggestions; to Professor Y. Senoo for his kind guidance as the supervisor until his departure; to Professor P. G. Hill for his valuable suggestions; to Mr. M. Lefcort for his help in the flow observation study and many suggestions; to Mr. Dalton Baugh, Mr. Basil Kean and other members of the Gas Turbine Laboratory for their help in making probes and arranging the test apparatus; and to Mrs. Elizabeth Johnson for typing this report.

ABSTRACT

The influence of tip clearance on the lift distribution along a blade span was studied on linear compressor and turbine cascades. The wall boundary layer was removed by means of the image technique. The lift distribution in the span direction was found to be almost similar for both compressor and turbine cascades having the similar velocity diagrams. The lift acting on the blades increases toward the blade tip. The phenomena were explained theoretically by considering the velocity induced by tip vortices on the blade surface.

SYMBOLS

A aspect ratio

a radius, inches

b span, inches

C_l section lift coefficient

C_n section normal-force coefficient

C_N normal-force coefficient of isolated airfoil

C_p pressure coefficient $\frac{p - p_1}{\frac{1}{2}\rho V_1^2}$

C_{x1} inlet axial velocity, feet per second

C_{x2} outlet axial velocity, feet per second

c blade chord, inches

F complex potential

P_o stagnation pressure, pounds per square foot

p pressure on blade surface, pounds per square foot

p_1 upstream pressure, pounds per square foot

R distance between point on surface and tip vortex line, inches

R_e Reynolds number

r distance between point on surface and tip vortex segment, inches

s distance from leading edge along tip vortex line, inches

u velocity in chord direction, feet per second

V_1 inlet velocity, feet per second

V_2 outlet velocity, feet per second

V_{2d} velocity around two-dimensional airfoil, feet per second

v velocity in span direction, feet per second

w velocity normal to blade surface, feet per second

w_o velocity w induced by tip vortices, feet per second

w_{tr} velocity w induced by trailing vortices, feet per second

X non-dimensional chordwise distance x/c

x chordwise distance, inches

Y non-dimensional spanwise distance y/c

y spanwise distance, inches

Y_o clearance to chord ratio, y_o/c

y_o tip clearance, inches

Z complex plane

z distance normal to blade surface, inches

α local incidence angle, degrees

α_1 incidence angle, degrees

α_2 outlet angle, degrees

α_∞ mean flow angle, degrees

β angle between blade surface and tip vortex line, degrees

γ circulation of bound vortex

Γ total circulation around profile

$\overline{\Gamma}$ non-dimensional circulation around profile

Γ_o circulation of tip vortex

$\overline{\Gamma}_o$ non-dimensional circulation of tip vortex

Γ_{2d} circulation around two-dimensional airfoil

$\overline{\Gamma}_n$ Fourier coefficient

ζ complex plane

η spanwise distance, inches

λ stagger angle, degrees

ξ chordwise distance, inches

ρ fluid density, slugs per cubic foot

1. INTRODUCTION

It is well known that the amount of tip clearance has a large effect on the performance of axial flow machines. The results obtained by past experiments show different trends from compressor to compressor [1] and it seems to be difficult to obtain a generalized expression for the effect of tip clearance.

The flow phenomenon in the vicinity of a blade tip in an axial flow machine may be considered as a combination or an interaction of phenomena due to three different causes, i.e., the amount of tip clearance, the boundary layer on the annulus wall and the relative blade tip velocity to the wall. To study the problem in detail, an experiment was conducted by G. Khabbaz [2] in the Gas Turbine Laboratory in 1959. In this experiment, the tip clearance effect on stall limit of compressor cascades was studied using the image method to eliminate the wall boundary layer. He found through the test that

1) stall occurred at a higher angle of attack near the wing tip than for the remainder of the blade,

2) as the clearance size is increased, the loading on the blade near the tip increases, while at a greater distance from the tip it remains unchanged.

He explained the phenomena by applying the momentum theory to a control volume taken between the blade tips as shown in the figure.

net momentum flux out = $(p_1 - p_2)$ x Area

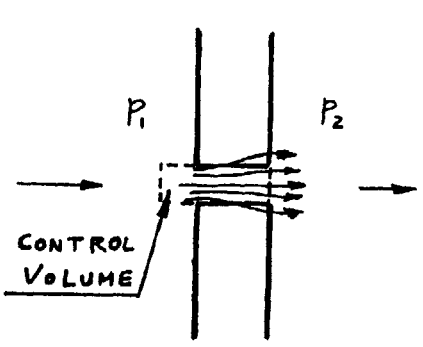

For compressor cascades, the pressure at the outlet of the blade row p_2 is higher than the inlet pressure p_1, and the momentum flux coming into the

control volume must be larger than that going out from it. Accordingly, some air must leave the cascade by passing through the blade row to satisfy the continuity. Since the flow at a greater distance from the tip is two-dimensional, this flow will increase the local velocity near the tip and result in an increase of the lift near the blade tip.

If this hypothesis is correct, then the reverse result must be obtained for turbine cascades because the pressure at the inlet of the turbine cascade is higher than that at the exit.

The experiment was continued by the authro to check this effect. After the cascade test, it was thought that it was necessary to observe the flow near the tip for understanding the phenomena in more detail, and flow observation was attempted by using tufts in the cascade and by the ink tracing method in a water table.

The problem is also treated theoretically in this report.

2 Description of Test Apparatus

2.1 Low Speed Wind Tunnel Cascade

The experiments were carried on the same apparatus used by G. Khabbaz. The cascade consists of nine blades; four of them were cut in halves to make the clearance (Fig. 1).

The dimensions of the cascade are given in Table 1.

Table 1 Dimensions of the cascade

Blade Profile	NACA 65-410	
Chord Length	$c = 4.875$ in.	
Solidity	$\sigma = 1.0$	
Clearance to Chord Ratio	$Y_o = y_o/c = .03$	
	Compressor	Turbine
Stagger Angle	$\lambda = 55°$	$= -59°$
Air Inlet Angle	$\alpha_1 = 65°$	$= 54°$
Air Inlet Velocity	$V_1 = 110$ Ft/Sec	$= 70$ Ft/Sec
Reynolds Number*	$R_e = 2.8 \times 10^5$	$= 1.8 \times 10^5$

(*) Based on inlet velocity and chord length

The blade surface pressure was measured by two blades in the middle of the cascade. The pressure taps on these blades are located along the chord at various distances from the blade tip as shown in Table 2. Static pressures were fed into a multi-tube inclined manometer by vinyl tubes.

Table 2 Position of Static Pressure Taps on Blade Surface

Chordwise Distance from Leading Edge (percent chord)

No.	1	2	3	4	5	6	7	8	9	10	11	12	13	14	15
Distance	2.5	5.0	7.5	10	20	30	40	50	60	70	75	80	85	90	95

Spanwise Distance from Blade Tip, inches

No.	1	2	3	4	5	6	7	8
Distance	1/16	3/16	7/16	11/16	15/16	$1^{11}/16$	$2^{11}/16$	$4^{11}/16$

2.2 Probes

A pitot static tube was placed at a chord length upstream of the blade row for measuring the inlet velocity and pressure. The flow downstream of the blade row was measured by traversing a five-hole probe in a plane at a chord length downstream of trailing edges of the blades. The pressure tubes from the probe were connected to a wire strain gauge type transducer and the pressures were read by a D.C. balancing bridge type calibrator.

3 Test Results

Fig. 2 shows the pressure distribution on the blade surface of the compressor cascade. It can be seen from the figure that the static pressure on the suction surface decreases considerably as the blade tip is approached, but there is little change in pressure on the pressure surface.

The static pressure on the suction surface at different chords were plotted against the distance from the blade tip in Fig. 3. The region influenced due to the tip clearance is spread toward the trailing edge along the chord except in the vicinity of the leading edge.

The outlet axial velocity obtained by the wake traverse was divided by inlet axial velocity and plotted in Fig. 4. It shows a typical wake shape at y/c = 0.4, but for smaller values of y/c, the pattern deforms gradually and a highest velocity appears at downstream of the suction side and lowest velocity at downstream of the pressure side of the blade.

Fig. 5 shows the distributions of the mean axial velocity, the turning angle and the lift coefficient along the span. The mean value of the outlet axial velocity and the lift coefficient were obtained by integrating curves in Fig. 4 and Fig. 2 respectively. The turning angle was calculated by using continuity and momentum equations assuming that no mixing occurrs in the spanwise direction. The outlet axial velocity and the turning angle decrease toward the tip in spite of the increase in the lift coefficient.

Surface pressure measurements were also made for a turbine cascade. The stagger angle in this case was so chosen that the velocity diagrams for compressor and turbine cascades are similar.

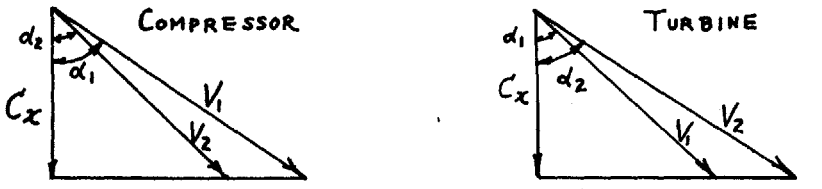

$\alpha_1)_{\text{comp.}} = \alpha_2)_{\text{tur.}}$, $\alpha_2)_{\text{comp.}} = \alpha_1)_{\text{tur.}}$

The surface pressure distribution is shown in Fig. 6, and the non-dimensional lift coefficient is plotted in Fig. 7 together with the results obtained from the compressor cascade. The trend is almost the same for both cascades.

4 Discussion of Test Results

The test results may be summarized as follows:

(1) For the compressor cascade, the turning angle and the outlet

axial velocity decrease near the blade tip in spite of the increase in the lift coefficient.

(2) For both compressor and turbine cascades, the lift coefficient increases toward the tip.

These phenomena cannot be explained by the momentum theory which was applied to this problem by Khabbaz.

Before entering the discussion of the tip clearance effect, let us look at the flow around a single wing of finite aspect ratio. There are some reports concerning the lift or pressure distribution along the span of wings of small aspect ratio.[3],[4] Fig. 8 is one of the test results obtained by Holme. The lifting surface theory shows the correct behavior for very small angles of incidence. However, as the angle of attack is increased, the loading becomes larger near the tip. Except at small angles, the lifting surface theory gives very inaccurate results even for angles of attack much smaller than the stalling angle.

To investigate the flow phenomena near a wing tip in detail, flow was observed by tufts in the wind tunnel and also by the ink tracing method in a water table. In the experiments, a strong wing tip vortex was observed as shown in Fig. 9. Air rolls up around the wing tip and makes a wing tip vortex above the suction surface. This tip vortex will have a large influence on the blade surface pressure, especially on the suction surface since the vortices exist above the suction surface. To confirm the effect of tip vortices on the surface pressure, a crude calculation was attempted under the following assumptions.

1. Velocity on the blade surface is approximately the sum of velocities induced by two-dimensional bound vortices and tip vortices,

the effect of trailing vortices are neglected since the strength of trailing vortices were observed to be much smaller than that of the tip vortices.

2. The distribution of the bound vortices along a chord is approximated by a linear function of x/c, because the circulation of a bound vortex is proportional to the pressure difference between the surfaces, and the pressure difference would be approximated by a triangle as shown in the figure.

——— ACTUAL PRESSURE

— - - — APPROXIMATED

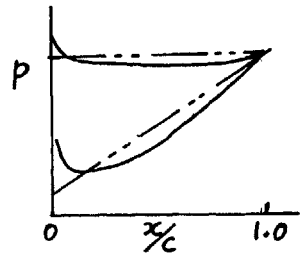

Figure 10

3. The tip vortices are a continuation of the bound vortices and exist in the x-z plane (Fig. I-3) with an angle β to the x-y plane.

Two different assumptions were made to express the position of the tip vortices.

i) The wing tip vortices leave from the wing tip parallel to each other. (Fig. I-3-i)

ii) The wing tip vortices leave from the wing tip and join a vortex which started from the leading edge with an angle to the blade surface. (Fig. I-3-ii)

In both cases, the angle β was approximated as equal to the angle between the chord line and mean flow direction, that is

$$\beta = \alpha_\infty - \lambda = \tan^{-1}\left(\frac{\tan\alpha_1 + \tan\alpha_2}{2}\right) - \lambda$$

The pressure on the suction surface at y/c = .0385 was evaluated by taking images of the tip vortices to satisfy the boundary condition on the surface (see Appendix I).

$V_z = 0$, on surface (x,y,0)

The result was plotted in Fig. 11. The pressure distribution along the span was also calculated at $x/c = 0.5$, and shown in Fig. 12. The pressure distribution calculated by the assumption (3-ii) shows comparatively good agreement with the test result. We will be able to say from the figures that the assumptions made for the calculation are not far from the actual flow phenomena. However, the procedure used here, i.e. the use of the image vortices to satisfy the boundary condition is not applicable in evaluating pressures on the pressure surface.

In the lifting surface theory,[7] this boundary condition was satisfied by the relation

$$w + V_1 \operatorname{Sin} \alpha_1 = 0. \qquad (1)$$

That is, the normal component of the induced velocity cancels the normal component of inlet flow.

The problem may be solved by using Eq. 1 as the boundary condition and the calculation procedure will be similar to that for the lifting surface theory, the only difference is that the equation would involve additional terms due to the tip vortices which were not considered in the original lifting surface theory.

The treatment of the problem as a lifting surface will be much more complicated and a laborious numerical calculation will be required to solve it. If our main interest is to know the distribution of lift in the span direction, this complication may be avoided by means of the lifting line approximation. The procedure will be shown in the following chapter.

5 Modified Lifting-Line Theory

5.1 Single Flat Plate Wing

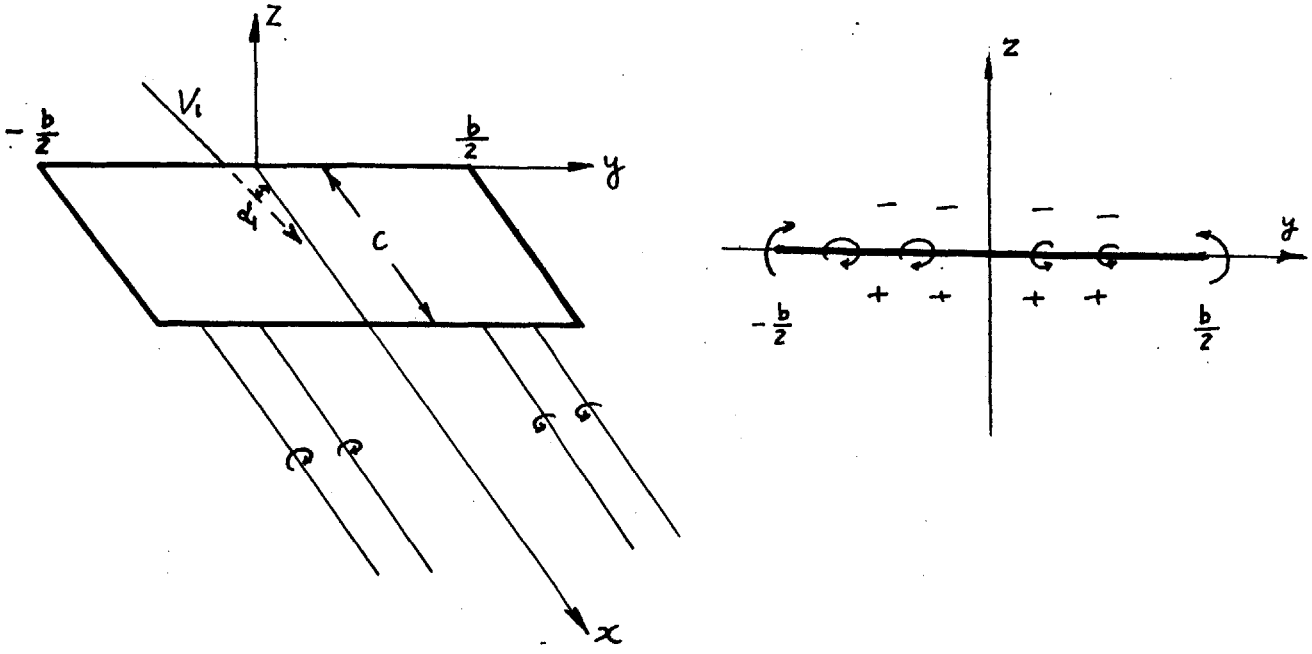

Figure 13

Consider a flat rectangular wing placed in a free stream of velocity V_1 with a small angle of attack α_1. Some air flows from the bottome to the top around the wing tips due to the pressure difference between the surfaces, and trailing vortices are formed from the trailing edge of the wing as explained by Prandtl.[6] However, as the angle of attack α_1 is increased, the pressure difference between the surface increases, consequently a strong upward flow appears around the tips, which rolls up above the suction surface and forms wing tip vortices as shown in Fig. 14. The wing tip vortices

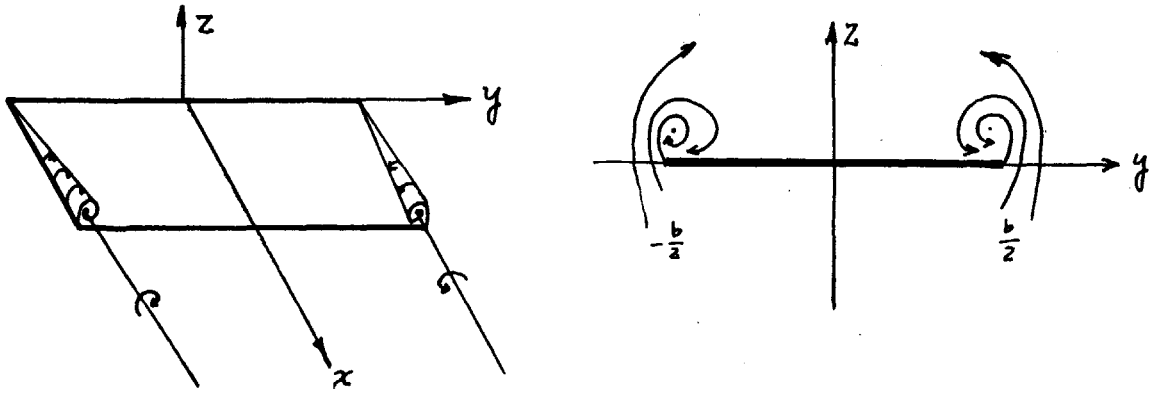

Figure 14

induce velocity in the direction from the center of the span to the wing tips, the magnitude of which is approximately inversely proportional to the distance between the vortex and the point on the surface and proportional to the cosine of the angle δ shown in Figure 15.

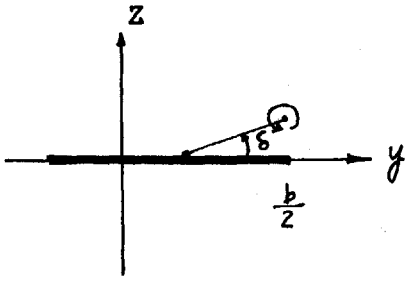

Figure 15

The interesting thing is that the direction of this induced velocity is opposite to that in the Prandtl hypothesis.

In the Prandtl theory, the trailing vortices were considered as the continuation of the bound vortices and the system was replaced by a set of horseshoe vortices (fig. 16). If the same assumption is made for the present case, i.e. the wing tip vortices and the trailing vortices are considered as the continuation of the bound vortices, then the system will be as shown in Fig. 17.

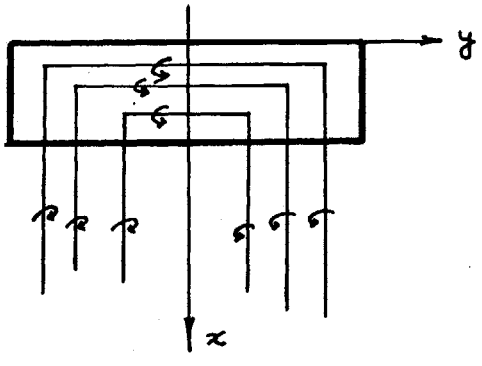

Figure 16 Prandtl's Hypothesis

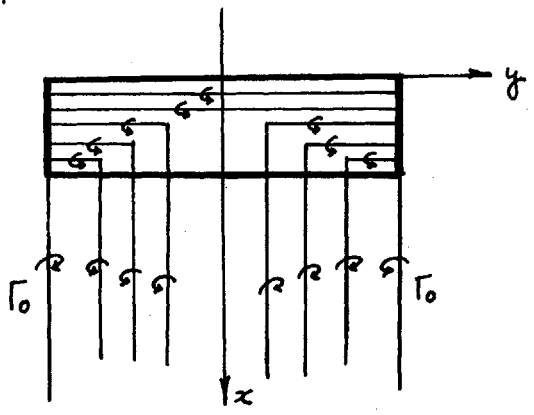

Figure 17 Present Case

It can be seen from Fig. 17 that the total circulation $\Gamma(y)$ around the profile increases toward the tip and at the tip it has a finite value which is equal to the circulation of the wing tip vortices Γ_0.

Lifting Line Approximation

For the wing of large aspect ratio, A = b/c $\gg$ 1, the system in Fig. 17 may be simplified to the system shown in Fig. 18; the wing is replaced by a vortex of circulation $\Gamma(y)$ which is an unknown function of y.

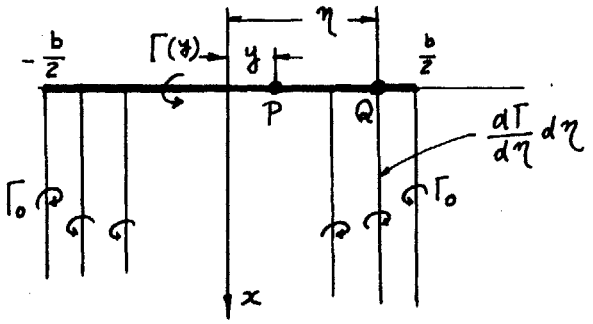

Figure 18

The induced velocity at a point P(0,y) is the sum of velocities induced by the tip vortices and the trailing vortices, since a bound vortex induces no velocity at its own center.

Applying Biot-Savart's law (Eq. I-4) to the system, the velocity induced by the tip vortices which extend from x = 0 to x = ∞ is given by

$$w_0 = -\frac{\Gamma_0}{4\pi}\left(\frac{1}{\frac{b}{2}-y} - \frac{1}{\frac{b}{2}+y}\right) = -\frac{\Gamma_0}{2\pi}\frac{\frac{b}{2}}{\left(\frac{b}{2}\right)^2 - y^2} \cdot \quad (2)$$

The negative sign in the equation means that the induced velocity is in the negative z-direction.

The velocity induced by a trailing vortex of circulation $\frac{d\Gamma}{d\eta}d\eta$ through the point Q $(0, \eta)$ is

$$dw_{tr} = \frac{\frac{d\Gamma}{d\eta}}{4\pi(\eta - y)}d\eta \ . \quad (3)$$

Integrating Eq. 3 along the span, we get the induced velocity due to all the trailing vortices

$$w_{tr} = \frac{1}{4\pi}\int_{-\frac{b}{2}}^{\frac{b}{2}} \frac{\frac{d\Gamma}{d\eta}}{\eta - y}d\eta \ . \quad (4)$$

Thus, the total induced velocity at P (0,y) becomes

$$w = w_o + w_{tr} = -\frac{\Gamma_o}{2\pi}\frac{\frac{b}{2}}{(\frac{b}{2})^2 - y^2} + \frac{1}{4\pi}\int_{-\frac{b}{2}}^{\frac{b}{2}} \frac{\frac{d\Gamma}{d\eta}}{\eta - y}\, d\eta \quad (5)$$

The total circulation around the profile is expressed as (see Appendix II)

$$\Gamma(y) = \pi c V_1 \sin\alpha = \pi c V_1 \sin(\alpha_1 + \frac{w}{V_1}) \quad (6)$$

For a small angle of attack, $\sin\alpha \cong \alpha$, then

$$\Gamma(y) = \pi c V_1 (\alpha_1 + \frac{w}{V_1}) = \pi c V_1 \alpha_1 + \pi c w \quad (7)$$

Substituting Eq. 4 into Eq. 7, we obtain

$$\Gamma(y) = \pi c V_1 \alpha_1 - \frac{c\Gamma_o}{2}\left[\frac{\frac{b}{2}}{(\frac{b}{2})^2 - y^2}\right] + \frac{c}{4}\int_{-\frac{b}{2}}^{\frac{b}{2}} \frac{\frac{d\Gamma}{d\eta}}{\eta - y}\, d\eta \quad (8)$$

The first term of the equation is equivalent to the circulation of a two-dimensional wing, that is the circulation around a wing of infinite aspect ratio, so we define

$$\Gamma_{2d} \equiv \pi c V_1 \alpha_1 \quad (9)$$

Dividing Eq. 8 by Eq. 9, we get

$$\bar{\Gamma}(y) = 1 - \frac{c}{2}\bar{\Gamma}_o\left[\frac{\frac{b}{2}}{(\frac{b}{2})^2 - y^2}\right] + \frac{c}{4}\int_{-\frac{b}{2}}^{\frac{b}{2}} \frac{\frac{d\bar{\Gamma}}{d\eta}}{\eta - y}\, d\eta \quad (10)$$

where

$$\bar{\Gamma}(y) \equiv \frac{\Gamma(y)}{\Gamma_{2d}}, \qquad \bar{\Gamma}_o \equiv \frac{\Gamma_o}{\Gamma_{2d}}.$$

The variables y and η may be changed into θ and ϕ by the following relations

$$\left.\begin{aligned} y &= -\frac{b}{2}\cos\theta, \qquad \eta = -\frac{b}{2}\cos\phi, \\ \bar{\Gamma}(y) &= \bar{\Gamma}(-\tfrac{b}{2}\cos\theta) = \bar{\Gamma}'(\theta). \end{aligned}\right\} \quad (11)$$

Combining these equations, the non-dimensional expression is obtained.

$$\bar{\Gamma}'(\theta) = 1 - \frac{\bar{\Gamma}_0}{A}\left(\frac{1}{1-\cos^2\theta}\right) - \frac{1}{2A}\int_{\phi=0}^{\phi=\pi} \frac{d\bar{\Gamma}'(\phi)}{\cos\phi - \cos\theta} \tag{12}$$

where A = aspect ratio = b/c.

Assume $\bar{\Gamma}'(\theta)$ may be represented by the function

$$\bar{\Gamma}'(\theta) = \bar{\Gamma}_0 + \sum_{n=1}^{\infty} \bar{\Gamma}_n \sin n\theta \tag{13}$$

since $\bar{\Gamma}'(\theta)$ has a finite value at $\theta = 0$ and $\theta = \pi$.

Noting that n must be an odd integer to ensure the equality

$$\sin n\theta = \sin n(\pi - \theta),$$

n is taken as

$$n = 2m + 1, \quad m = 0, 1, 2, 3, \ldots \tag{14}$$

Substituting Eqs. 13 and 14 into Eq. 12, we get

$$\bar{\Gamma}_0 + \sum_{m=0}^{\infty} \bar{\Gamma}_{(2m+1)} \sin(2m+1)\theta = 1 - \frac{\bar{\Gamma}_0}{A}\frac{1}{1-\cos^2\theta} - \frac{1}{2A}\sum_{m=0}^{\infty} \bar{\Gamma}_{(2m+1)} \int_0^{\pi} \frac{\cos(2m+1)\phi}{\cos\phi - \cos\theta} d\phi \tag{15}$$

Evaluating the integral on the right hand side and noting that the point $\theta = \phi$ must be omitted since a vortex induces no velocity at its own center,[5]

$$\int_0^{\pi} \frac{\cos(2m+1)\phi}{\cos\phi - \cos\theta} d\phi = \lim_{\varepsilon \to 0}\left[\int_0^{\theta-\varepsilon} \frac{\cos(2m+1)\phi}{\cos\phi - \cos\theta} d\phi + \int_{\theta+\varepsilon}^{\pi} \frac{\cos(2m+1)\phi}{\cos\phi - \cos\theta} d\phi\right]$$

$$= \pi \frac{\sin(2m+1)\theta}{\sin\theta}.$$

Therefore, it follows that

$$1 = \bar{\Gamma}_0\left[1 + \frac{1}{A}\frac{1}{1-\cos^2\theta}\right] + \sum_{m=0}^{\infty} \bar{\Gamma}_{(2m+1)}\left[1 + \frac{\pi}{2A}\frac{2m+1}{\sin\theta}\right]\sin(2m+1)\theta$$

or

$$1 = \bar{\Gamma}_0\left[1 + \frac{1}{2A}\left(\frac{1}{1-\cos\theta} + \frac{1}{1+\cos\theta}\right)\right] + \sum_{m=0}^{\infty} \bar{\Gamma}_{(2m+1)}\left[1 + \frac{\pi}{2A}\frac{2m+1}{\sin\theta}\right]\sin(2m+1)\theta. \tag{16}$$

The coefficients $\overline{\Gamma}_0$ and $\overline{\Gamma}_{(2m+1)}$ can be evaluated approximately by taking a finite number of particular values of θ . For $\theta = 0$, the term $1/(1-\cos\theta)$ in Eq. 16 must be set equal to zero for the same reason described in evaluating theintegral of Eq. 15.

The theory developed above will be useful for evaluating the lift distribution along the span for wings of large aspect ratio, since the theory was derived based on the lifting line approximation.

As an example, the distribution of normal-force coefficient for a wing of aspect ratio 6 was calculated by locating θ at 0, 30, 60, and 90 degrees.

The normal-force coefficient C_n was divided by the mean value of C_n, that is

$$C_N = \frac{1}{b}\int_{-\frac{b}{2}}^{\frac{b}{2}} C_n \, dy \quad ,$$

and the result was plotted in Fig. 19. The curve shows the correct trend at the region near the wing tip.

5.2 Tip Clearance Effect

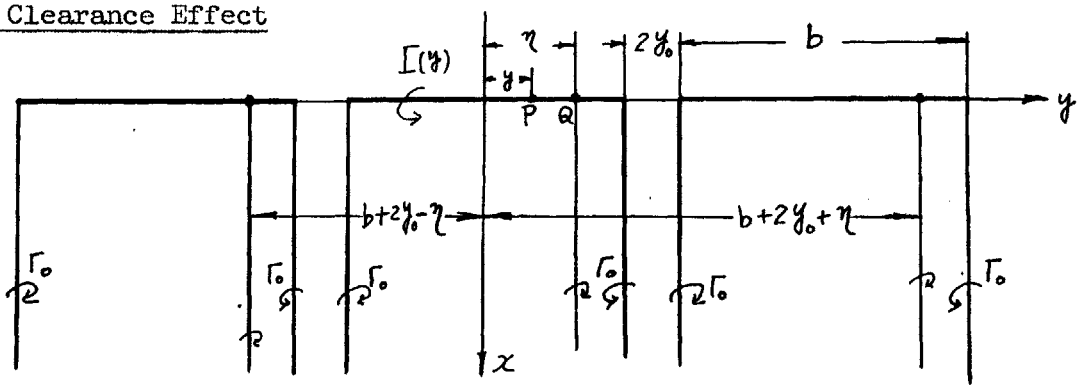

Figure 20

Place three blades in a plane with clearances $2y_0$ between the adjacent blades.*

---

* 1. First an attempt was made to solve the problem for two blades of semi-infinite span. However, the solution was found to diverge since the wing span extended to infinity. This trouble may be avoided by

The induced velocity at a point P (0,y) can be evaluated by the same manner as in the previous calculation.

Velocity induced by tip vortices;

$$w_0 = -\frac{\Gamma_0}{4\pi}\left[\frac{1}{(\frac{b}{2})-y} + \frac{1}{(\frac{b}{2})+y} + \frac{1}{\frac{3}{2}b+2y_0-y} + \frac{1}{\frac{3}{2}b+2y_0+y} - \frac{1}{\frac{b}{2}+2y_0-y} - \frac{1}{\frac{b}{2}+2y_0+y}\right]$$

$$= -\frac{\Gamma_0}{2\pi}\left[\frac{\frac{b}{2}}{(\frac{b}{2})^2-y^2} + \frac{2y_0+\frac{3}{2}b}{(2y_0+\frac{3}{2}b)^2-y^2} - \frac{2y_0+\frac{b}{2}}{(2y_0+\frac{b}{2})^2-y^2}\right] \quad (17)$$

Velocity induced by trailing vortices;

$$w_{tr} = \frac{1}{4\pi}\int_{-\frac{b}{2}}^{\frac{b}{2}}\left[\frac{\frac{d\Gamma}{d\eta}}{\eta-y} + \frac{\frac{d\Gamma}{d\eta}}{b+2y_0+\eta-y} - \frac{\frac{d\Gamma}{d\eta}}{b+2y_0+y-\eta}\right]d\eta \quad (18)$$

Substituting Eqs. 17 and 18 into Eq. 7, we get the expression for the distribution of circulation along the span.

$$\Gamma(y) = \pi c V_1 \alpha_1 - \frac{c\Gamma_0}{2}\left[\frac{\frac{b}{2}}{(\frac{b}{2})^2-y^2} + \frac{2y_0+\frac{3}{2}b}{(2y_0+\frac{3}{2}b)^2-y^2} - \frac{2y_0+\frac{b}{2}}{(2y_0+\frac{b}{2})^2-y^2}\right] + \frac{c}{4}\int_{-\frac{b}{2}}^{\frac{b}{2}}\frac{d\Gamma}{d\eta}\left[\frac{1}{\eta-y} + \frac{1}{b+2y_0+\eta-y} - \frac{1}{b+2y_0+y-\eta}\right]d\eta \quad (19)$$

Changing the variables by the relations

$$y = -\frac{b}{2}\cos\theta \quad , \quad \eta = -\frac{b}{2}\cos\phi \quad , \qquad (20)$$

and using the non-dimensional expressions

$$\bar{\Gamma}(y) \equiv \frac{\Gamma(y)}{\Gamma_{2d}} \quad , \quad \bar{\Gamma}_0 \equiv \frac{\Gamma_0}{\Gamma_{2d}} \quad ,$$

---

solving the problem for long blades but finite span.

2. Three blades were taken instead of two, so that the lift distribution along the span can be considered as symmetric to x axis and the calculation would be much simplified.

$$\left.\begin{aligned} \bar{\Gamma}(y) &= \bar{\Gamma}\left(-\tfrac{b}{2}\cos\theta\right) \equiv \bar{\Gamma}'(\theta) \quad , \\ \frac{b}{c} &= A \quad , \quad \frac{y_0}{c} \equiv Y_0 \end{aligned}\right\} \tag{21}$$

Eq. 19 becomes as follows:

$$\bar{\Gamma}'(\theta) = 1 - \frac{\bar{\Gamma}_0}{A}\left[\frac{1}{1-\cos^2\theta} + \frac{3+4Y_0/A}{(3+4Y_0/A)^2-\cos^2\theta} - \frac{1+4Y_0/A}{(1+4Y_0/A)^2-\cos^2\theta}\right]$$

$$- \frac{1}{2A}\int_{\phi=0}^{\phi=\pi}\left[\frac{1}{\cos\phi-\cos\theta} + \frac{1}{(2+4Y_0/A-\cos\theta)+\cos\phi} - \frac{1}{(2+4Y_0/A+\cos\theta)-\cos\phi}\right]d\phi \tag{22}$$

Again $\bar{\Gamma}'(\theta)$ is assumed as

$$\bar{\Gamma}'(\theta) = \bar{\Gamma}_0 + \sum_{m=0}^{\infty} \bar{\Gamma}_{(2m+1)} \sin(2m+1)\theta \quad , \tag{23}$$

and then,

$$d\bar{\Gamma}'(\phi) = \sum_{m=0}^{\infty} (2m+1)\bar{\Gamma}_{(2m+1)} \cos(2m+1)\phi \; d\phi \; . \tag{24}$$

From Eq. 22, 23 and 24, we get

$$\bar{\Gamma}_0 + \sum_{m=0}^{\infty} \bar{\Gamma}_{(2m+1)} \sin(2m+1)\theta$$

$$= 1 - \frac{\bar{\Gamma}_0}{A}\left[\frac{1}{1-\cos^2\theta} + \frac{3+4Y_0/A}{(3+4Y_0/A)^2-\cos^2\theta} - \frac{1+4Y_0/A}{(1+4Y_0/A)^2-\cos^2\theta}\right]$$

$$- \frac{1}{2A}\sum_{m=0}^{\infty} (2m+1)\bar{\Gamma}_{(2m+1)}\left[I_{1,m} + I_{2,m} - I_{3,m}\right] \quad , \tag{25}$$

where

$$I_{1,m} = \int_0^{\pi} \frac{\cos(2m+1)\phi}{\cos\phi - \cos\theta}\, d\phi = \pi \frac{\sin(2m+1)\theta}{\sin\theta} \quad ,$$

$$I_{2,m} = \int_0^{\pi} \frac{\cos(2m+1)\phi}{K_1 + \cos\phi}\, d\phi \quad ,$$

$$I_{3,m} = \int_0^{\pi} \frac{\cos(2m+1)\phi}{K_2 - \cos\phi}\, d\phi \quad ,$$

and
$$\left.\begin{aligned} K_1 &= 2 + 4\,Y_0/A - \cos\theta > 1 \\ K_2 &= 2 + 4\,Y_0/A + \cos\theta > 1 \end{aligned}\right\} \text{ for } 0 \le \theta \le \pi \ .$$

The solution of integrals $I_{2,m}$ and $I_{3,m}$ cannot be expressed in simple forms like that of $I_{1,m}$. Here, the integrals were evaluated step by step and the following equation was obtained:

$$\begin{aligned} I = {} & \bar{\Gamma}_0 \left\{ 1 + \frac{1}{A}\left[\frac{1}{1-\cos^2\theta} + \frac{3 + 4\,Y_0/A}{(3+4\,Y_0/A)^2 - \cos^2\theta} - \frac{1 + 4\,Y_0/A}{(1+4\,Y_0/A)^2 - \cos^2\theta} \right] \right\} \\ & + \bar{\Gamma}_1 \left\{ \sin\theta + \frac{\pi}{2A}\left[3 - \frac{K_1}{\sqrt{K_1^2 - 1}} - \frac{K_2}{\sqrt{K_2^2 - 1}} \right] \right\} \\ & + \bar{\Gamma}_3 \left\{ \sin 3\theta + \frac{\pi}{2A}\left[\frac{\sin 3\theta}{\sin\theta} + 4(K_1^2 + K_2^2) - 2 - \frac{K_1(4K_1^2 - 3)}{\sqrt{K_1^2 - 1}} - \frac{K_2(4K_2^2 - 3)}{\sqrt{K_2^2 - 1}} \right] \right\} \\ & + \bar{\Gamma}_5 \left\{ \sin 5\theta + \frac{\pi}{2A}\left[\frac{\sin 5\theta}{\sin\theta} + 16(K_1^4 + K_2^4) - 12(K_1^2 + K_2^2) + 2 \right.\right. \\ & \qquad \left.\left. - \frac{K_1(16K_1^4 - 20K_1^2 + 5)}{\sqrt{K_1^2 - 1}} - \frac{K_2(16K_1^4 - 20K_1^2 + 5)}{\sqrt{K_2^2 - 1}} \right] \right\} \\ & + \text{------} \end{aligned} \tag{26}$$

The equation may be useful for wings of large aspect ratio and with comparatively large tip clearance. A numerical calculation was tried for A = 10 and Y_0 = 0.1, and the result was compared in Fig. 21 with the test result obtained by Khabbaz.

6. CONCLUSION

It can be concluded from the results obtained by the cascade tests that:

1) For a compressor cascade, the lift coefficient increases near the blade tip in spite of the decrease in the turning angle and the outlet axial velocity.

2) For the turbine cascade, the lift distribution in the spanwise direction shows a trend similar to that for the compressor cascade.

The problem was approached theoretically by considering a simplified vortex system, and the pressure distribution on the suction surface was calculated from the induced velocity due to the tip vortices. It shows a fairly good agreement with the test result.

Appendix I Evaluation of Static Pressure on Suction Surface

(1) Biot-Savart's Law

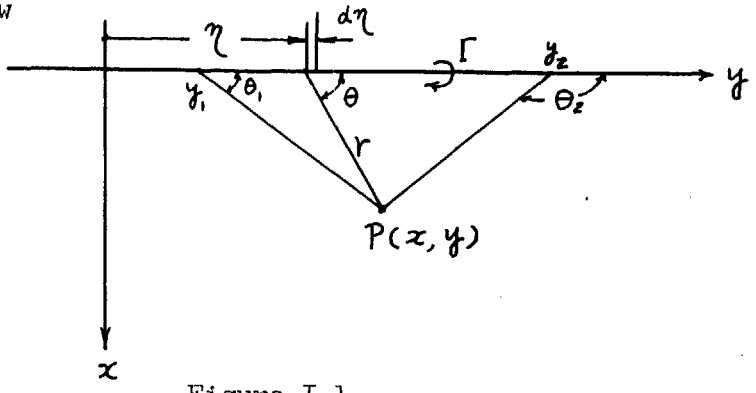

Figure I-1

If a vortex filament of circulation Γ lies in a plane, the velocity induced at point P(x,y) by the vortex segment ($y_1 \leq y \leq y_2$) can be evaluated by the law of Biot-Savart.

$$w = -\frac{\Gamma}{4\pi}\int_{y_1}^{y_2} \frac{\sin\theta}{r^2}\, d\eta \tag{I-1}$$

Considering the angle θ as the variable, we have

$$\left.\begin{aligned} y-\eta &= x\cot\theta\ , \qquad d\eta = \frac{x}{\sin^2\theta}\, d\theta \\ \text{and} \qquad r &= \frac{x}{\sin\theta}\ . \end{aligned}\right\} \tag{I-2}$$

Thus,

$$w = -\frac{\Gamma}{4\pi x}\int_{\theta_1}^{\theta_2} \sin\theta\, d\theta = \frac{\Gamma}{4\pi x}(\cos\theta_2 - \cos\theta_1)\ . \tag{I-3}$$

If the vortex filament extends to $y = +\infty$, then $\theta_2 = \pi$, $\cos\theta_2 = -1$, and the above expression becomes

$$w = -\frac{\Gamma}{4\pi x}(1+\cos\theta_1)\ . \tag{I-4}$$

(2) Circulation of Bound Vortex

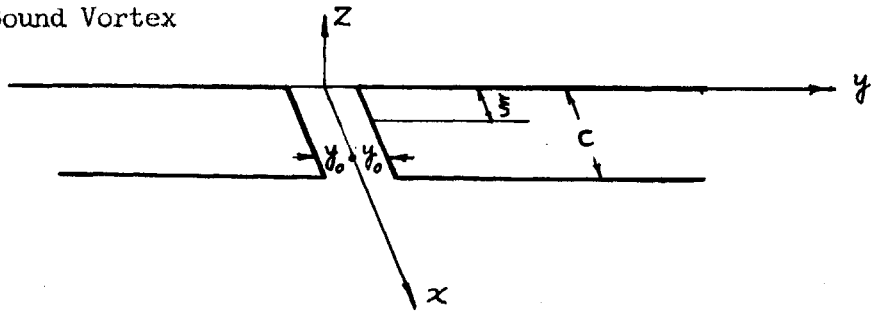

Figure (I-2)

According to the assumption (2) on page 7 , the circulation of a bound vortex at $x = \xi$ would be expressed as

$$\gamma(\xi) = \frac{\gamma_0 (c-\xi)}{c} = \gamma_0 \left(1 - \frac{\xi}{c}\right) . \tag{I-4}$$

Integrating this equation along the chord, we obtain the total circulation around the profile.

$$\int_0^c \gamma(\xi)\, d\xi = \gamma_0 \int_0^c \left(1 - \frac{\xi}{c}\right) d\xi = 2\gamma_0 c \equiv \Gamma_{2d} \tag{I-5}$$

or

$$\gamma_0 = \frac{2\Gamma_{2d}}{c}$$

where Γ_{2d} is the circulation around a two-dimensional wing according to the assumption (1) on page 6 .

Substituting Eq. I-5 into Eq. I-4, we get

$$\gamma(\xi) = \frac{2\Gamma_{2d}}{c}\left(1 - \frac{\xi}{c}\right) . \tag{I-6}$$

(3) Induced Velocity at P(x,y,o)

To satisfy the boundary condition on the surface, that is

$w = 0$, on P (x,y,0)

the images of the tip vortices are considered as shown in Fig. I-3.

Case (i)

The velocity at point P(x,y,0), induced by the tip vortices which leave from the wing tips at $x = \xi$ is expressed as (see Fig. I-4)

$$-dv = \frac{(x-\xi)\,\gamma(\xi)\,\sin\beta}{2\pi}\left[\frac{1+\cos\theta_1}{R_1^2} - \frac{1+\cos\theta_2}{R_2^2}\right]d\xi \qquad \text{(I-7)}$$

where

$$\left.\begin{aligned} R_1^2 &= (x-\xi)^2\sin^2\beta + (y-y_0)^2 \\ R_2^2 &= (x-\xi)^2\sin^2\beta + (y+y_0)^2 \end{aligned}\right\} \qquad \text{(I-8)}$$

$$\left.\begin{aligned} \cos\theta_1 &= \frac{(x-\xi)\cos\beta}{\sqrt{(x-\xi)^2 + (y-y_0)^2}} \\ \cos\theta_2 &= \frac{(x-\xi)\cos\beta}{\sqrt{(x-\xi)^2 + (y+y_0)^2}} \end{aligned}\right\} \qquad \text{(I-9)}$$

Substituting Eqs. I-6, I-8 and I-9 into Eq. I-7, we obtain the equation for the induced velocity.

$$-v = \frac{\Gamma_{2d}}{\pi c^2}\int_0^c (x-\xi)(c-\xi)\sin\beta\left\{\frac{\sqrt{(x-\xi)^2+(y-y_0)^2} + (x-\xi)\cos\beta}{\left[(x-\xi)^2\sin^2\beta + (y-y_0)^2\right]\sqrt{(x-\xi)^2+(y-y_0)^2}}\right.$$

$$\left. - \frac{\sqrt{(x-\xi)^2+(y+y_0)^2} + (x-\xi)\cos\beta}{\left[(x-\xi)^2\sin^2\beta + (y+y_0)^2\right]\sqrt{(x-\xi)^2+(y+y_0)^2}}\right\} d\xi$$

Expanding the equation in partial fractions, we get

$$-v = \frac{\Gamma_{2d}\sin\beta}{\pi c^2}\left\{\int_0^c \frac{(x-\xi)(c-\xi)}{(x-\xi)^2\sin^2\beta + (y-y_0)^2}d\xi - \int_0^c \frac{(x-\xi)(c-\xi)}{(x-\xi)^2\sin^2\beta + (y+y_0)^2}d\xi\right.$$

$$+ \cos\beta\int_0^c \frac{(x-\xi)^2(c-\xi)}{\left[(x-\xi)^2\sin^2\beta + (y-y_0)^2\right]\sqrt{(x-\xi)^2+(y-y_0)^2}}d\xi$$

$$\left. - \cos\beta\int_0^c \frac{(x-\xi)^2(c-\xi)}{\left[(x-\xi)^2\sin^2\beta + (y+y_0)^2\right]\sqrt{(x-\xi)^2+(y+y_0)^2}}d\xi\right\} \qquad \text{(I-10)}$$

The integrations of Eq. I-10 were evaluated term by term and the following result was obtained.

$$-\frac{\pi c \sin\beta}{\Gamma_{2d}} v = \frac{1-X}{2} \ln\left\{\frac{\left[(1-X)^2 \sin^2\beta + (Y+Y_0)^2\right]\left[X^2 \sin^2\beta + (Y-Y_0)^2\right]}{\left[(1-X)^2 \sin^2\beta + (Y-Y_0)^2\right]\left[X^2 \sin^2\beta + (Y+Y_0)^2\right]}\right.$$

$$\left. \times \frac{\left[\rho_1 - X\cos\beta\right]\left[\rho_2 + X\cos\beta\right]\left[\rho_3 - (1-X)\cos\beta\right]\left[\rho_4 + (1-X)\cos\beta\right]}{\left[\rho_1 + X\cos\beta\right]\left[\rho_2 - X\cos\beta\right]\left[\rho_3 + (1-X)\cos\beta\right]\left[\rho_4 - (1-X)\cos\beta\right]} \right\}$$

$$+ \frac{Y-Y_0}{\sin\beta}\left\{\tan^{-1}\frac{\rho_3 \tan\beta}{Y-Y_0} - \tan^{-1}\frac{\rho_1 \tan\beta}{Y-Y_0} - \tan^{-1}\frac{X\sin\beta}{Y-Y_0} - \tan^{-1}\frac{(1-X)\sin\beta}{Y-Y_0}\right\}$$

$$- \frac{Y+Y_0}{\sin\beta}\left\{\tan^{-1}\frac{\rho_4 \tan\beta}{Y+Y_0} - \tan^{-1}\frac{\rho_2 \tan\beta}{Y+Y_0} - \tan^{-1}\frac{X\sin\beta}{Y+Y_0} - \tan^{-1}\frac{(1-X)\sin\beta}{Y+Y_0}\right\}$$

$$+ (1-X)\cos\beta \ln\frac{\left[\rho_1 + X\right]\left[\rho_4 - (1-X)\right]}{\left[\rho_2 + X\right]\left[\rho_3 - (1-X)\right]}$$

$$+ \cos\beta\left[\rho_1 - \rho_2 - \rho_3 + \rho_4\right], \qquad (I-11)$$

Where

$$\left.\begin{aligned} \rho_1 &= \sqrt{X^2 + (Y-Y_0)^2}\,, \\ \rho_2 &= \sqrt{X^2 + (Y+Y_0)^2}\,, \\ \rho_3 &= \sqrt{(1-X)^2 + (Y-Y_0)^2}\,, \\ \rho_4 &= \sqrt{(1-X)^2 + (Y+Y_0)^2}\,, \\ X &= x/c\,, \quad Y = y/c\,, \quad Y_0 = y_0/c\,. \end{aligned}\right\} \qquad (I-12)$$

Case (ii)

From the geometry in Fig. I-5 and Biot-Savert's law, the velocity induced at point P(x,y,0) by a vortex segment ds is formulated as follows:

$$-v = \frac{1}{2\pi}\int_0^\infty \frac{\Gamma_0(\xi)\,\sin\theta_1\,ds}{r_1^2}\cdot\frac{x\,\sin\beta}{R_1} - \frac{1}{2\pi}\int_0^\infty \frac{\Gamma_0(\xi)\,\sin\theta_2\,ds}{r_2^2}\cdot\frac{x\,\sin\beta}{R_1}$$

$$= \frac{1}{2\pi}\int_0^\infty \left[\frac{\Gamma_0(\xi)\,x\,\sin\beta}{r_1^3} - \frac{\Gamma_0(\xi)\,x\,\sin\beta}{r_2^3}\right] ds \qquad \text{(I-13)}$$

Circulation of the tip vortices $\Gamma_0(\xi)$ may be written as

$$\left.\begin{aligned} \Gamma_0(\xi) &= \int_0^\xi \gamma(\xi)\,d\xi = \gamma_0\int_0^\xi \left(1-\frac{\xi}{c}\right)d\xi = \frac{2\Gamma_{2d}}{c^2}(c\xi-\xi^2), \quad \text{for } (0\le\xi\le c), \\ \Gamma_0(\xi) &= \int_0^c \gamma(\xi)\,d\xi = \frac{c\gamma_0}{2} = \Gamma_{2d}, \quad \text{for } (\xi > c). \end{aligned}\right\} \qquad \text{(I-14)}$$

r_1, r_2 and ds are expressed in terms of x, ξ and R as follows.

$$\left.\begin{aligned} \cos\beta &= \frac{\xi}{s}, \qquad ds = \frac{d\xi}{\cos\beta}, \\ r_1 &= \sqrt{R_1^2 + (x\cos\beta - \xi\sec\beta)^2}, \\ r_2 &= \sqrt{R_2^2 + (x\cos\beta - \xi\sec\beta)^2}. \end{aligned}\right\} \qquad \text{(I-15)}$$

Substituting Eq. I-14 and Eq. I-15 into Eq. I-13, we get

$$-v = \frac{\Gamma_{2d}\,x}{\pi\,c^2}\tan\beta\int_0^c \left\{\frac{c\xi-\frac{\xi^2}{2}}{\left[R_1^2+(x\cos\beta-\xi\sec\beta)^2\right]^{3/2}} - \frac{c\xi-\frac{\xi^2}{2}}{\left[R_2^2+(x\cos\beta-\xi\sec\beta)^2\right]^{3/2}}\right\} d\xi$$

$$+ \frac{\Gamma_{2d}\,x}{2\pi}\tan\beta\int_0^c \left\{\frac{1}{\left[R_1^2+(x\cos\beta-\xi\sec\beta)^2\right]^{3/2}} - \frac{1}{\left[R_2^2+(x\cos\beta-\xi\sec\beta)^2\right]^{3/2}}\right\} d\xi$$

(I-16)

Integrating this and rearranging, we obtain the equation for the induced velocity at point P(x,y,0).

$$-\frac{2\pi c v}{X \Gamma_{2d} \sin\beta \cos^2\beta}$$

$$= (X\cos\beta - \sec\beta)\left\{\frac{3R_1'^2 + (x\cos\beta - \sec\beta)^2}{R_1'^2\sqrt{(x\cos\beta-\sec\beta)^2 + R_1'^2}} - \frac{3R_2'^2 + (X\cos\beta - \sec\beta)^2}{R_2'^2\sqrt{(x\cos\beta-\sec\beta)+R_2'^2}}\right\}$$

$$+ (2\sec\beta - X\cos\beta)\left[\frac{z_1}{R_1'^2} - \frac{z_2}{R_2'^2}\right]$$

$$+ \sec^2\beta\left[\frac{1}{R_1'^2} - \frac{1}{R_2'^2}\right]$$

$$+ \ln\frac{(X\cos\beta - \sec\beta) + \sqrt{(X\cos\beta - \sec\beta)^2 + R_1'^2}}{(x\cos\beta - \sec\beta) + \sqrt{(x\cos\beta - \sec\beta)^2 + R_2'^2}}$$

$$+ \ln\frac{X\cos\beta + z_2}{X\cos\beta + z_1} \qquad (I-17)$$

where

$$\left.\begin{aligned} R_1'^2 &= X^2\sin^2\beta + (Y - Y_0)^2 \\ R_2'^2 &= X^2\sin^2\beta + (Y + Y_0)^2 \end{aligned}\right\} \qquad (I-18)$$

The pressure coefficient on the blade surface was calculated as follows.

According to the assumption 1 in P. 6 , velocity on the blade surface is expressed as

$$\bar{V} = \bar{V}_{2d} + \bar{v} \quad ,$$

where $\bar{V}_{2d}$: velocity vector on a two-dimensional blade surface,

$\bar{v}$: velocity vector, induced by the tip vortices.

The magnitude of the velocity is

$$\bar{V} = \sqrt{\bar{V}_{2d}^2 + \bar{v}^2}$$

or

$$V^2 = V_{2d}^2 + v^2 \quad . \tag{I-19}$$

Bernoulli's equation for two-dimensional flow;

$$P_o = p_1 + (\rho/2)V_1^2 = p_{2d} + (\rho/2)V_{2d}^2$$

or

$$(p - p_1)_{2d} = (\rho/2)\,(V_1^2 - V_{2d}^2) \quad .$$

For three-dimensional cases, it becomes

$$p - p_1 = (\rho/2)(V_1^2 - V^2) = (\rho/2)(V_1^2 - V_{2d}^2) - (\rho/2)v^2$$
$$= (p - p_1)_{2d} - (\rho/2)v^2 \quad .$$

Dividing this equation by inlet dynamic pressure, we get the expression for the pressure coefficient.

$$C_p = \frac{p - p_1}{\frac{1}{2}\rho V_1^2} = C_p\Big)_{2d} - \frac{v^2}{V_1^2} \quad . \tag{I-20}$$

As an example, the pressure coefficients were calculated for the tested compressor blading using Eqs. I-20, I-11 and I-17. The results were plotted in Fig. 12 together with the test result.

Appendix II Circulation Around a Two-Dimensional Airfoil

The circulation around a wing of infinite aspect ratio can be obtained by means of the conformal mapping.

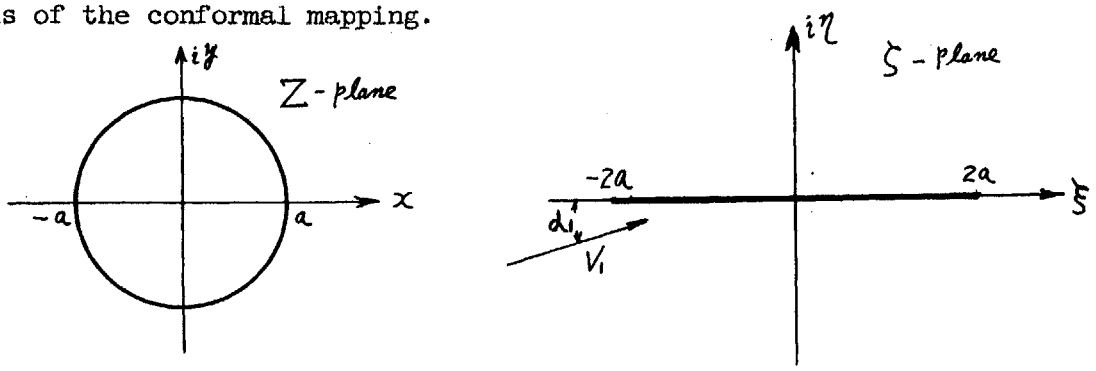

A circle of radius a given on the Z-plane is mapped into a straight line ($-2a \leq \xi \leq +2a$) in the ζ -plane by the function

$$\zeta = Z + \frac{a^2}{Z} \quad . \tag{II-1}$$

The complex potential of flow around the circle in the Z-plane is expressed as

$$F(Z) = V_1 e^{-i\alpha_1} Z + \frac{V_1 e^{i\alpha_1} a^2}{Z} + \frac{i\Gamma}{2\pi} \ln Z \quad . \tag{II-2}$$

Differentiating this equation with respect to Z, we get

$$\frac{dF}{dZ} = V_1 e^{-i\alpha_1} - \frac{V_1 e^{i\alpha_1} a^2}{Z^2} + \frac{i\Gamma}{2\pi Z} \quad . \tag{II-3}$$

The circulation Γ can be found from Eq. II-3 with the boundary condition

$$\frac{dF}{dZ} = 0 \quad , \qquad at \quad Z = a \quad . \tag{II-4}$$

Thus,

$$\Gamma = 4\pi a V_1 \sin\alpha_1 = \pi c V_1 \sin\alpha_1 \quad . \tag{II-5}$$

REFERENCES

1. McNair, R. E., "Tip Clearance Effects on Stalling Pressure Rise in Axial Flow Compressors" Westinghouse Electric Corporation, Lester Plant Steam Division Engineering Report E-1389, March, 1960.

2. Khabbaz, G. R., "The Influence of Tip Clearance on Stall Limits of a Rectilinear Cascade of Compressor Blades" Gas Turbine Laboratory Report No. 54, M.I.T., August 1959.

3. Winter, H., "Flow Phenomena on Plates and Airfoils of Short Span" NACA T.M. No. 798.

4. Holme, O.A.M., "Measurement of the Pressure Distribution on Rectangular Wings of Different Aspect Ratio" Flygtekniska Försöksanstalten, FFA No. 37, 1950.

5. Milne-Tomson, L.M., "Theoretical Aerodynamics", 3rd ed., p. 80, Macmillan and Co. Ltd., 1958.

6. Glauert, H., "The Elements of Airfoil and Airscrew Theory", Cambridge University Press, 1959.

7. Blenk, H., "Dew Eindecker als tragende Wirbelfläche", Z.a.M.M., Vol. 5, p. 36, 1925.

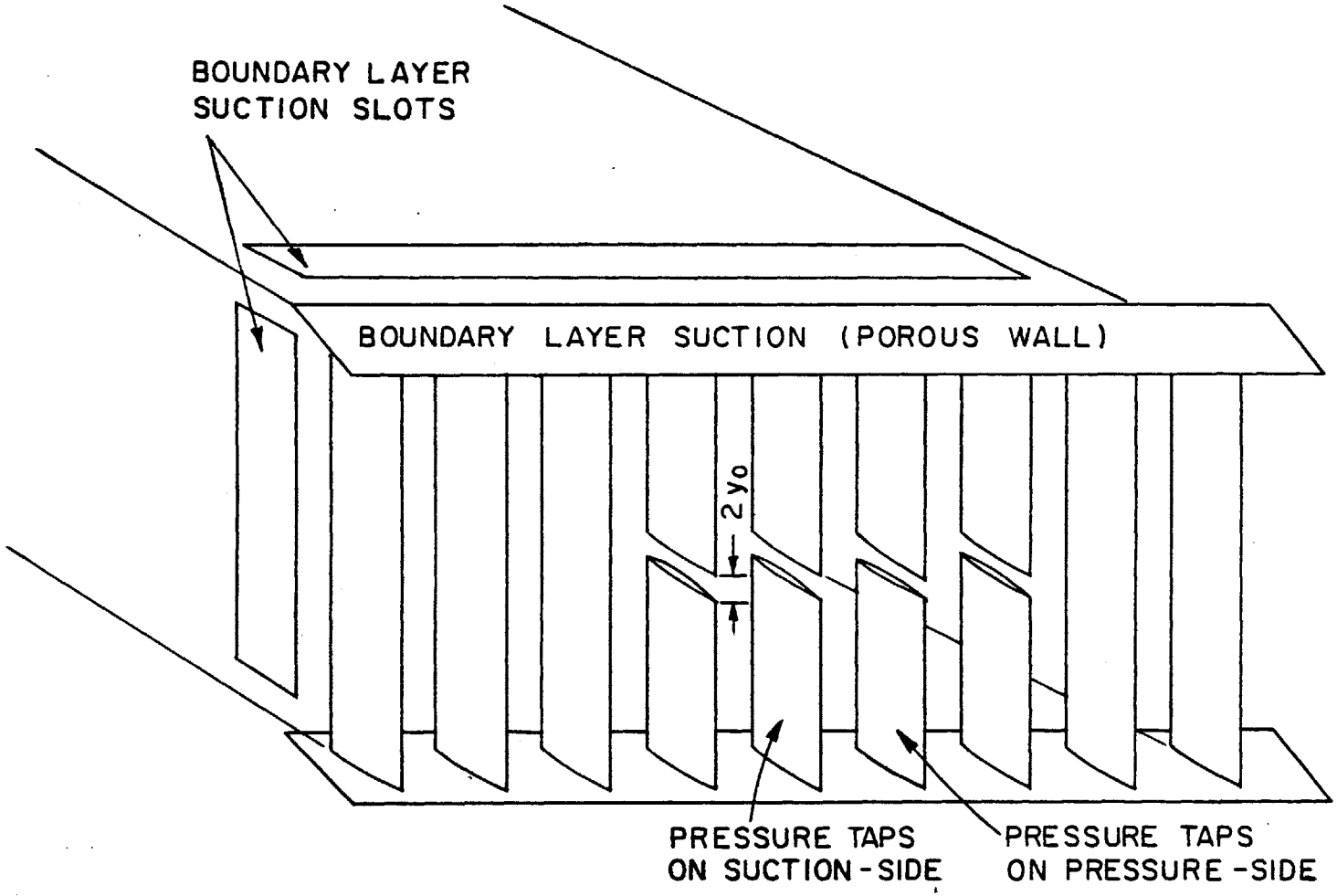

FIG. 1 LOW SPEED CASCADE

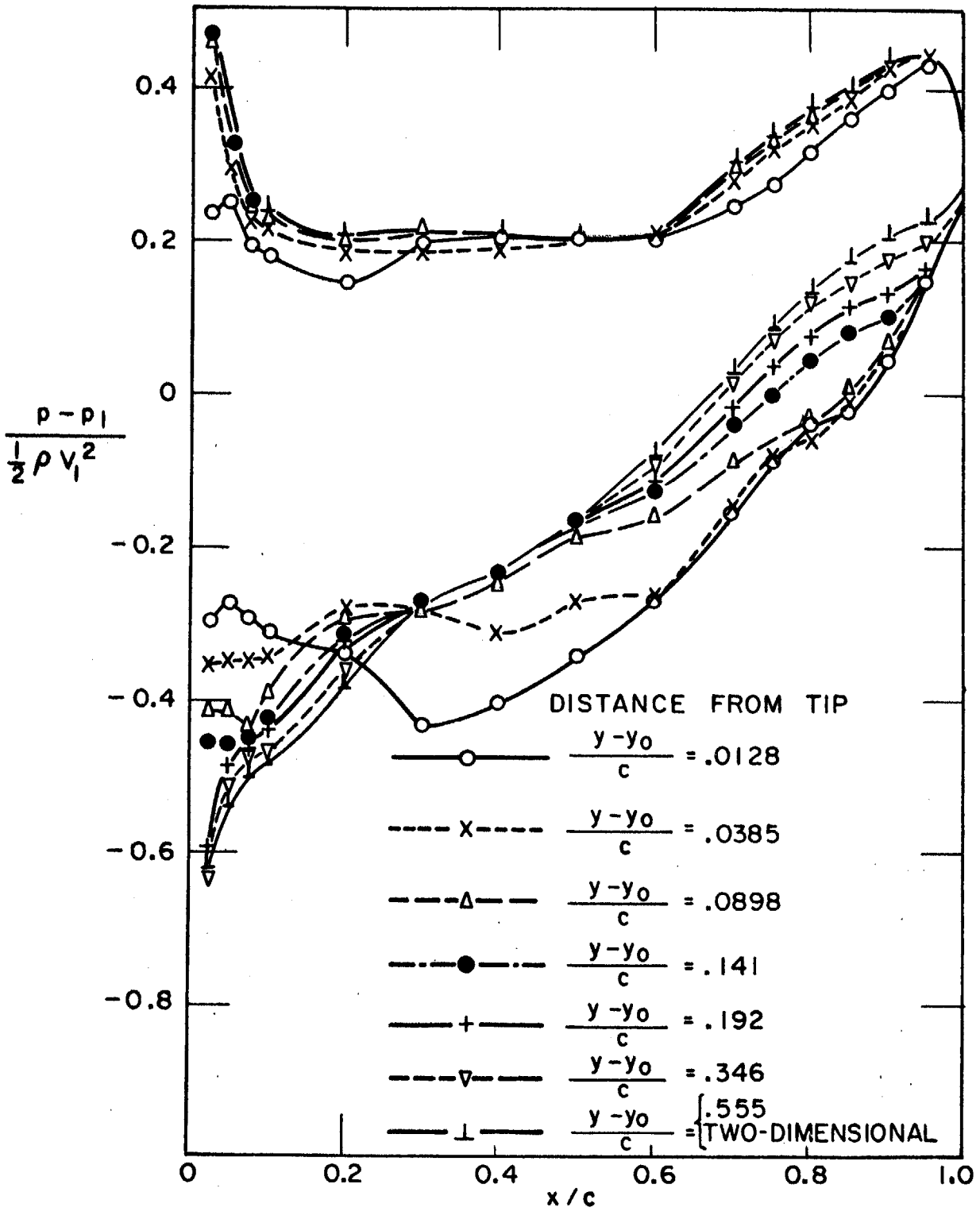

FIG. 2 PRESSURE DISTRIBUTION ON BLADE SURFACE OF A COMPRESSOR CASCADE

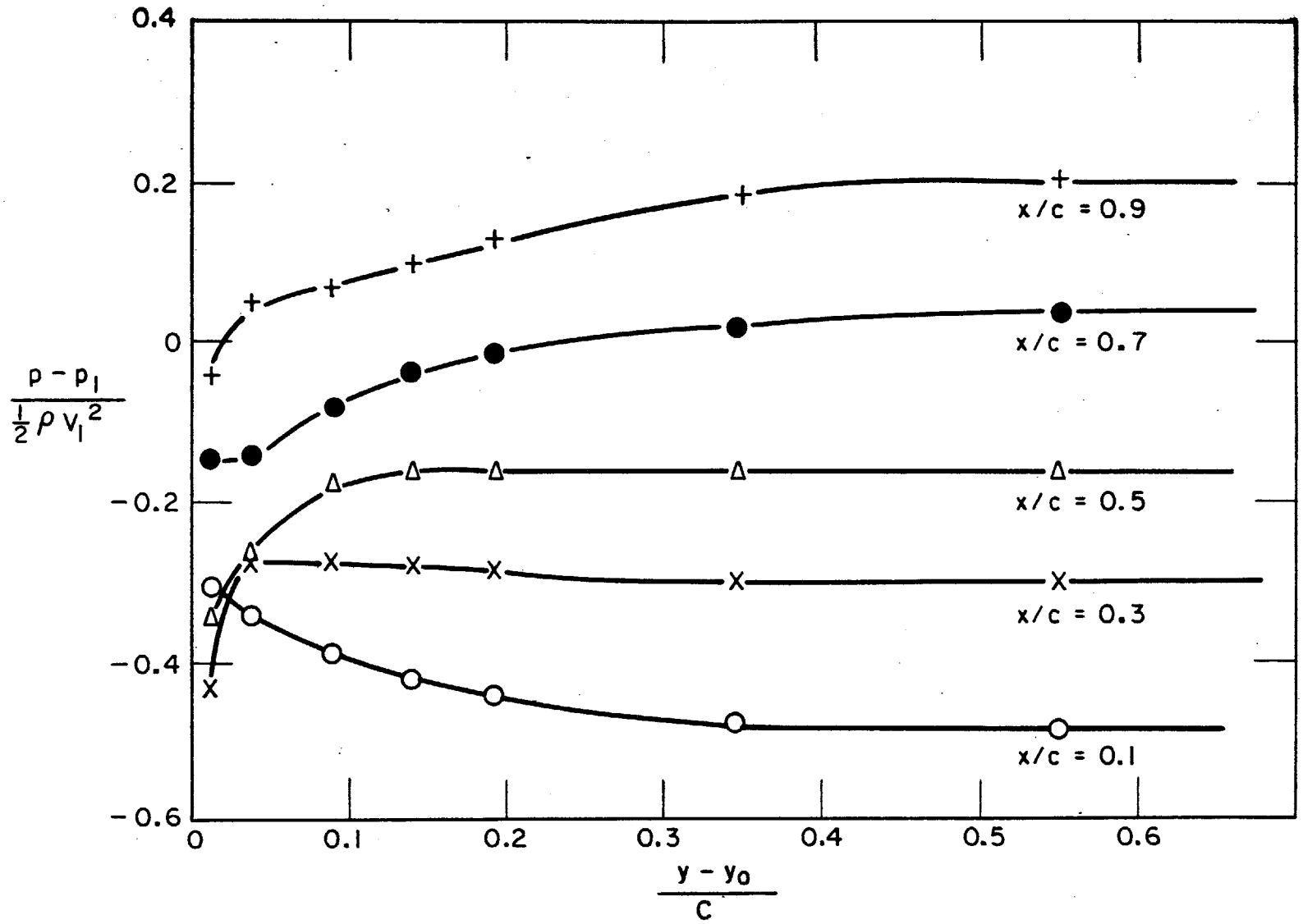

FIG. 3 BLADE SURFACE PRESSURE AT VARIOUS CHORDWISE DISTANCES VS. DISTANCE FROM TIP

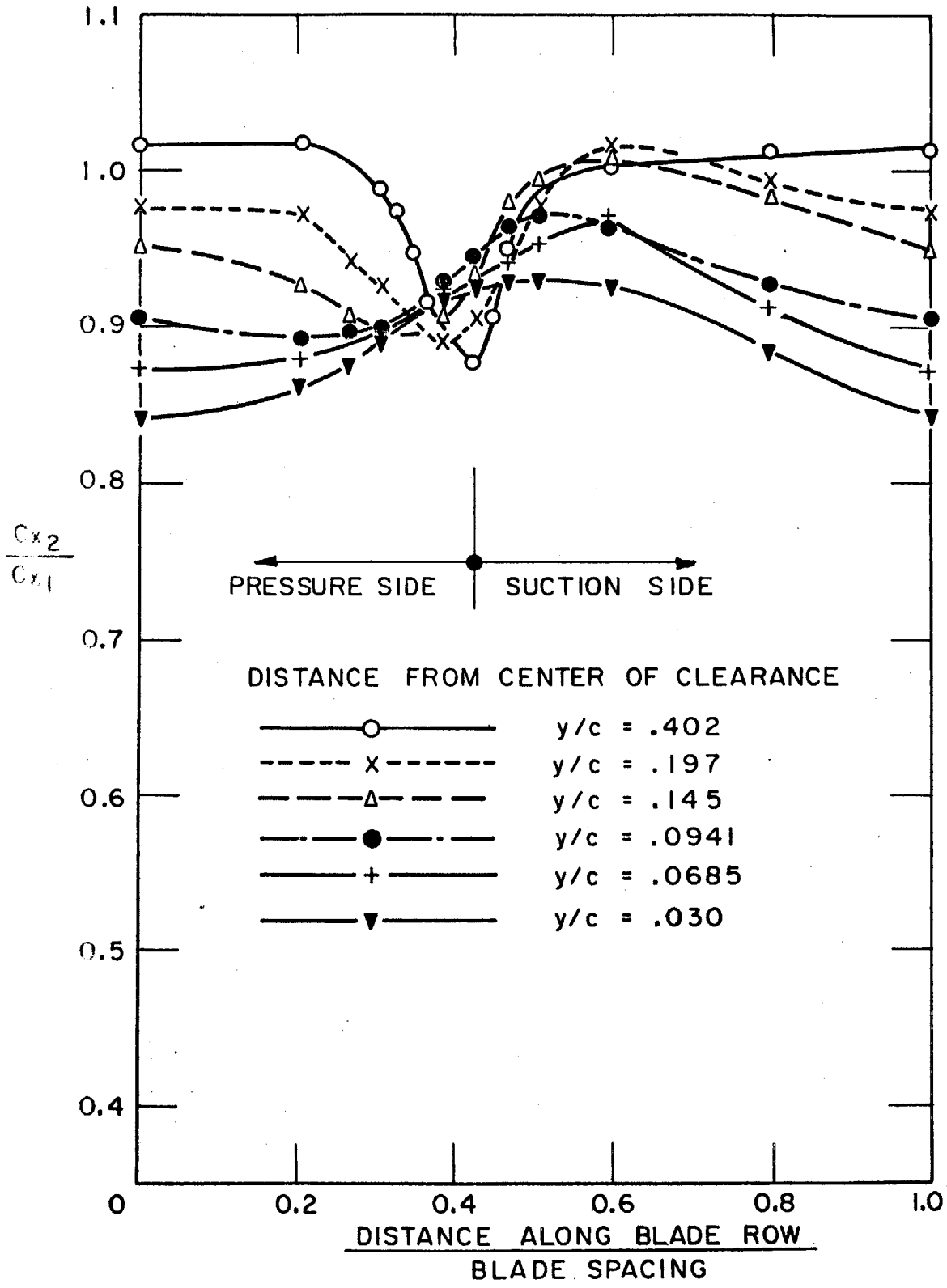

FIG. 4 DISTRIBUTION OF OUTLET AXIAL VELOCITY FOR COMPRESSOR CASCADE

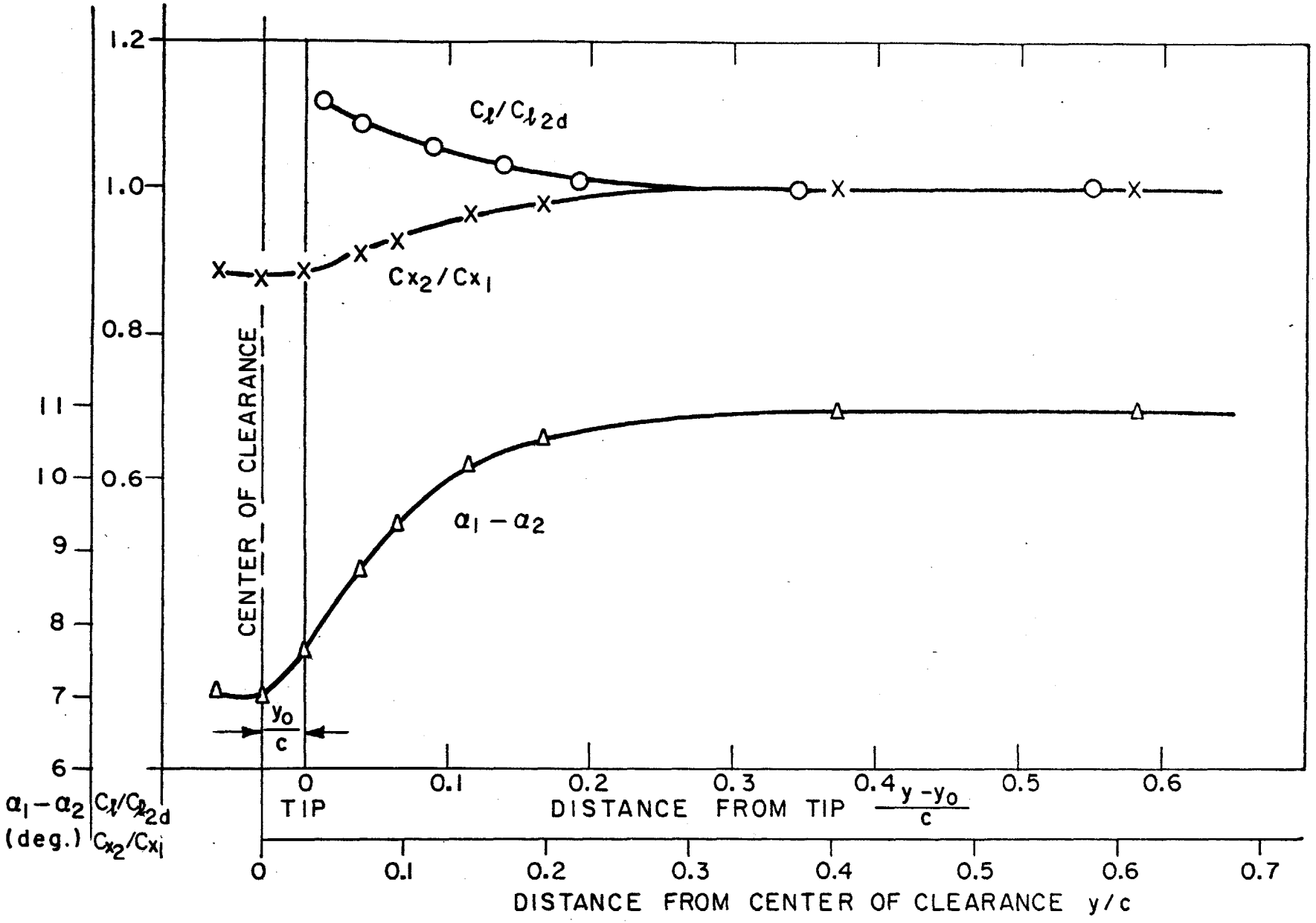

FIG. 5 DISTRIBUTIONS OF LIFT COEFFICIENT, OUTLET AXIAL VELOCITY AND TURNING ANGLE VS. SPANWISE DISTANCE

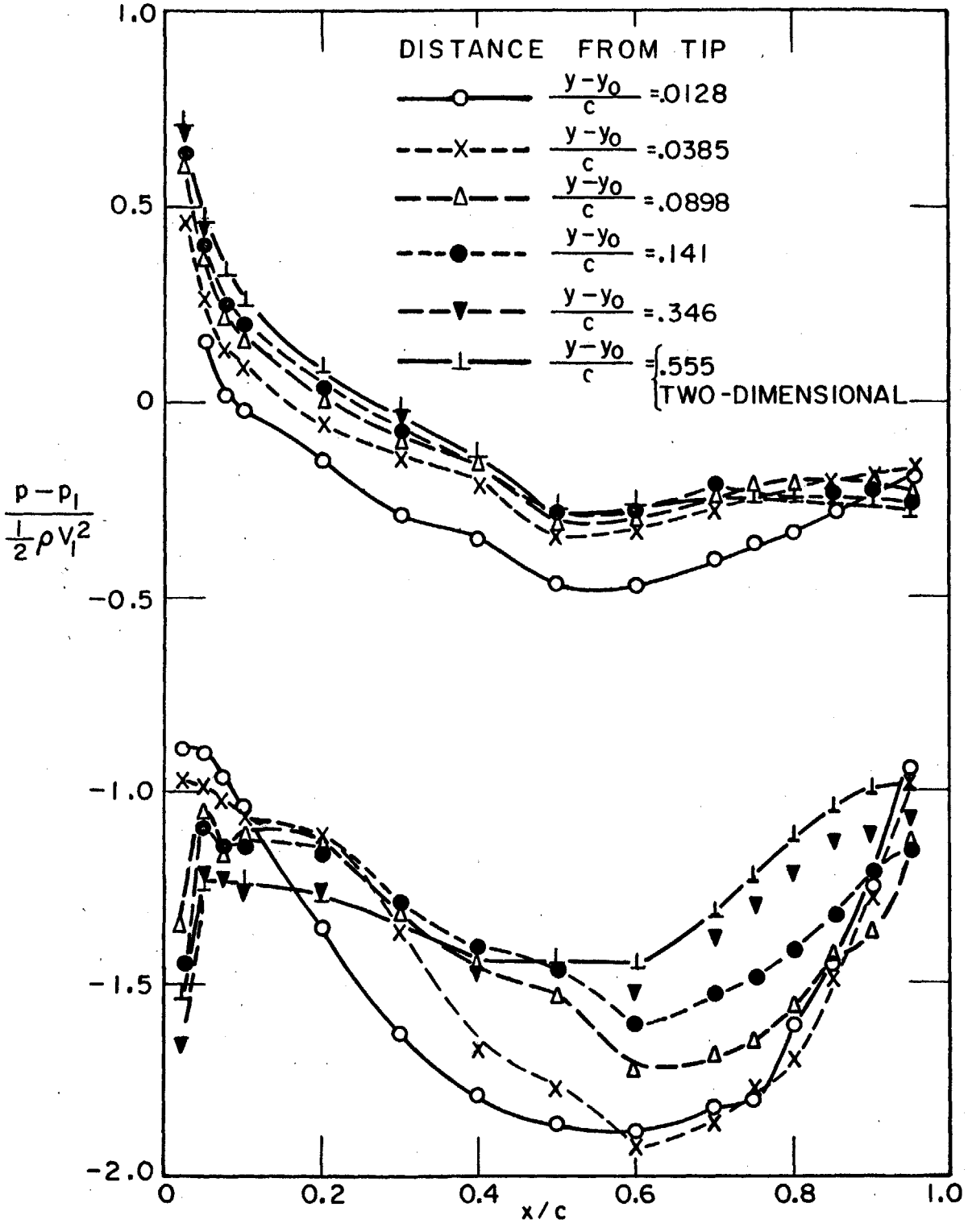

FIG. 6 PRESSURE DISTRIBUTION ON BLADE SURFACE OF TURBINE CASCADE

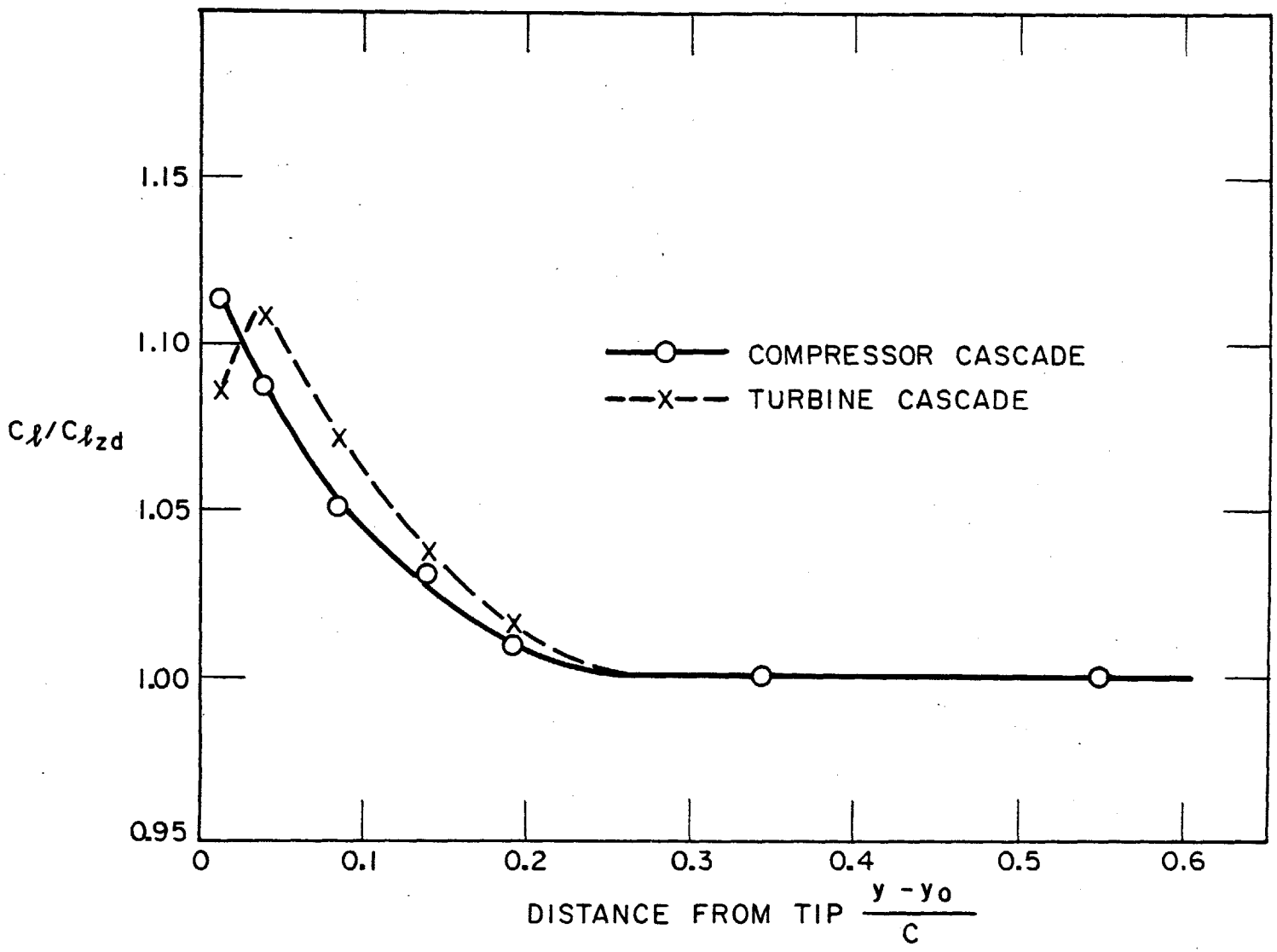

FIG. 7 COMPARISON OF LIFT DISTRIBUTION FOR TURBINE AND COMPRESSOR CASCADES

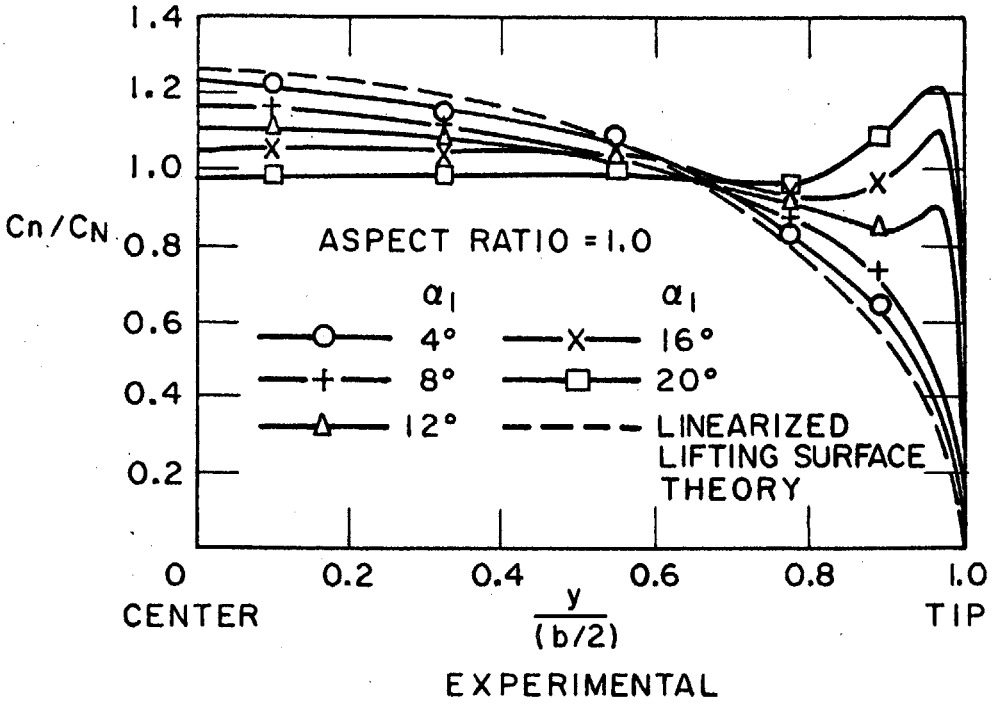

FIG. 8 NORMAL FORCE DISTRIBUTION ALONG SPAN OF RECTANGULAR WING OBTAINED BY HOLME

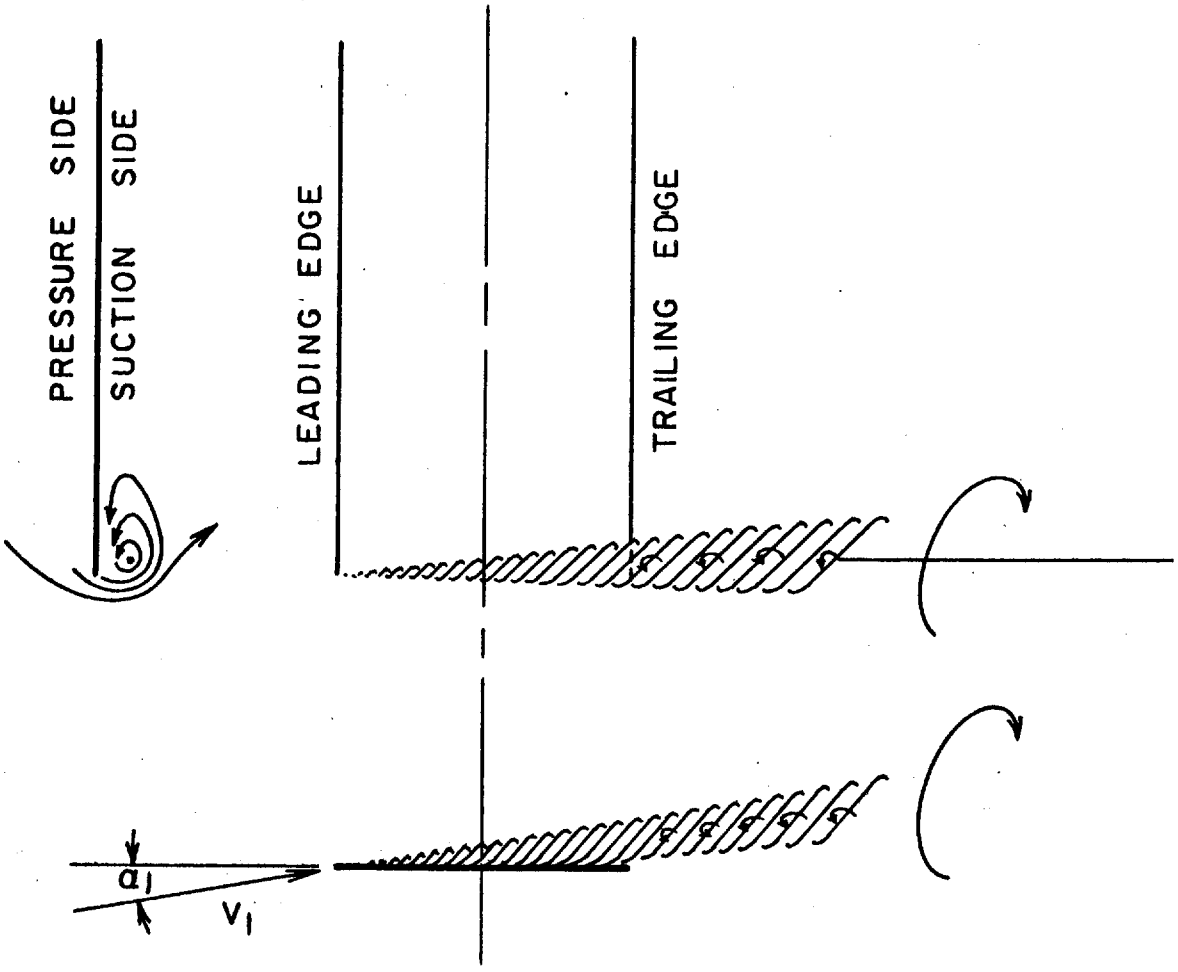

FIG.9 SKETCH OF WING TIP VORTEX

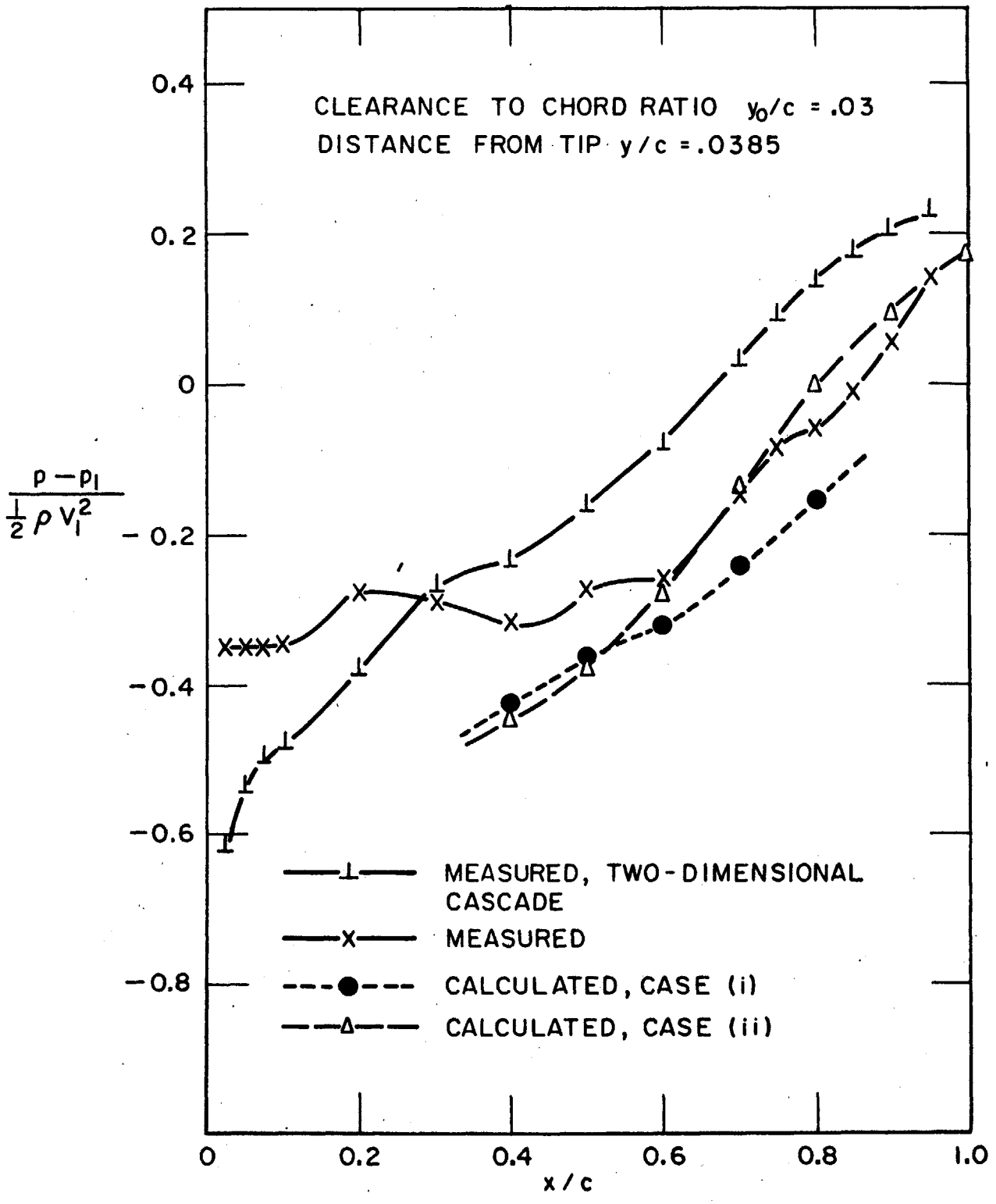

FIG. 11 PRESSURE DISTRIBUTION ON SUCTON SURFACE

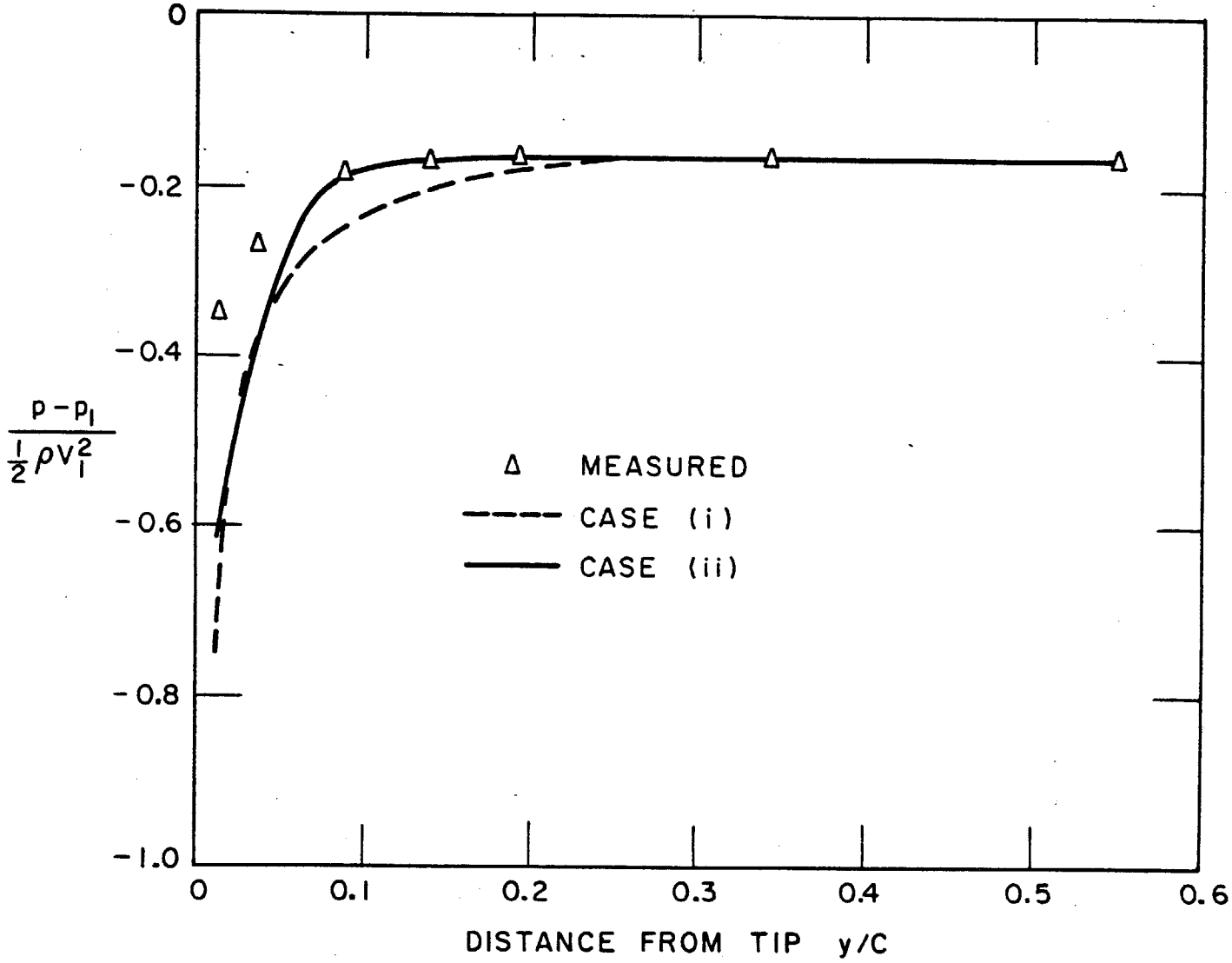

FIG. 12 PRESSURE DISTRIBUTION ALONG SPAN ON SUCTION SURFACE AT $x/\bar{c} = 0.5$

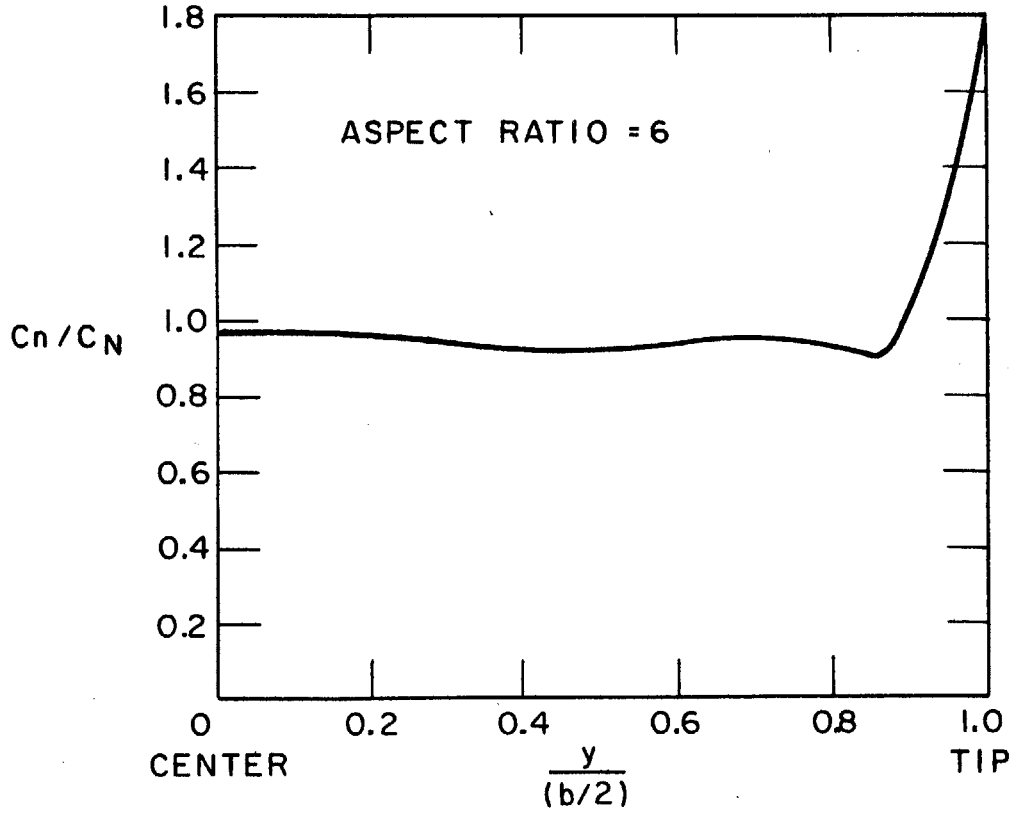

FIG. 19 CALCULATED NORMAL-FORCE DISTRIBUTION ALONG SPAN OF A RECTANGULAR WING

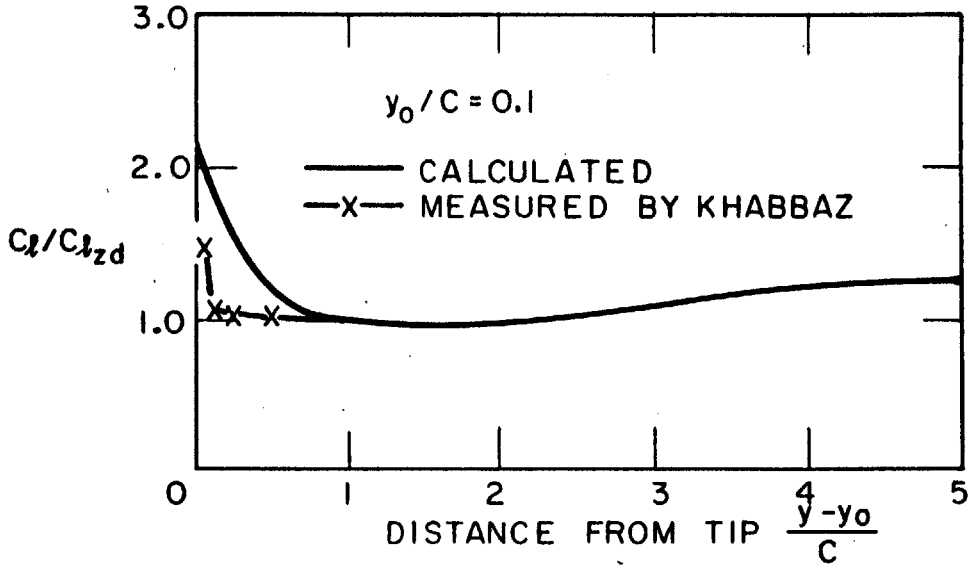

FIG. 21 DISTRIBUTION OF LIFE COEFFICIENT FOR A COMPRESSOR CASCADE WITH TIP CLEARANCE $y_0/C = 0.1$

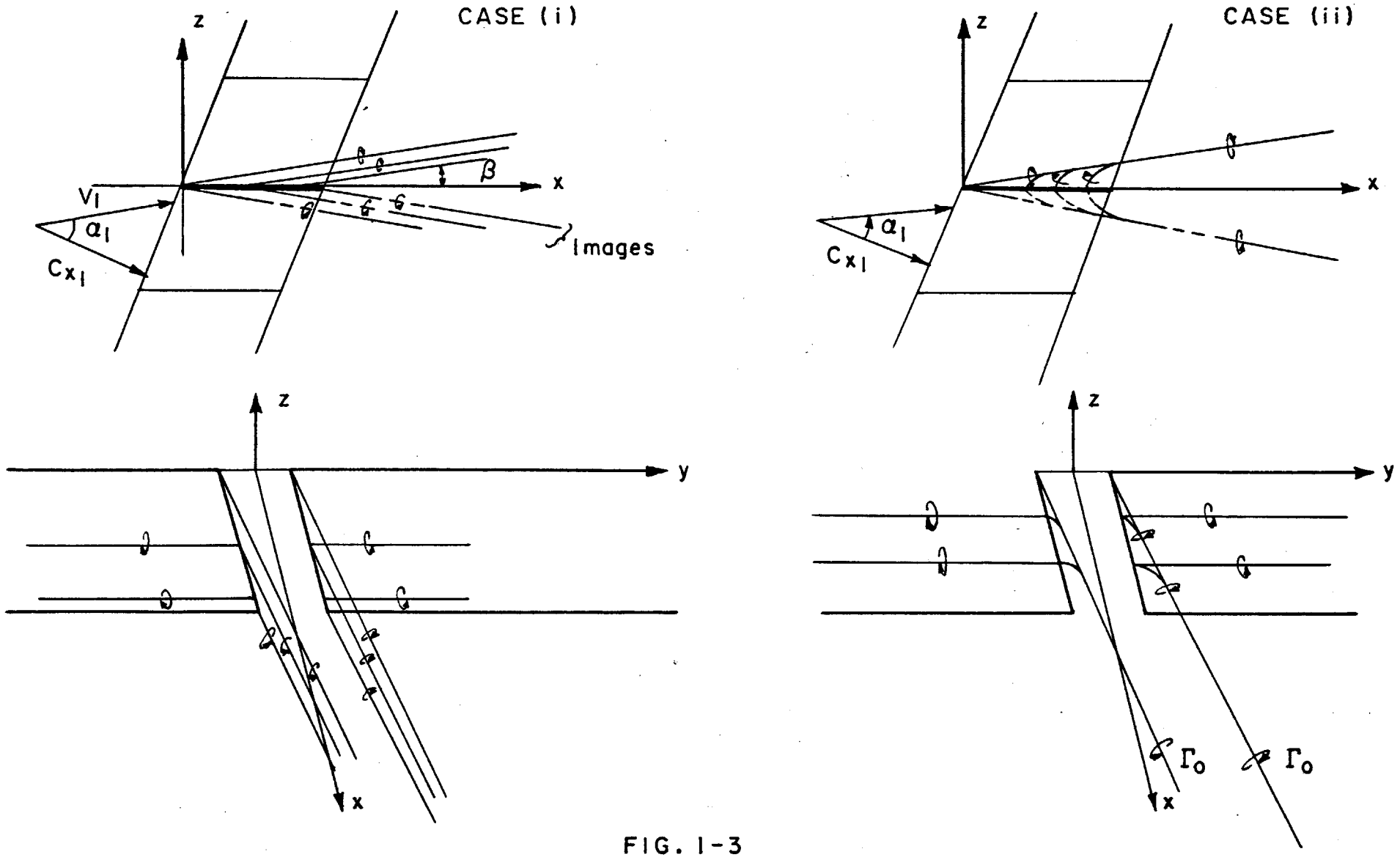
CASE (i)
z
x
β
V_1
α_1
C_{x_1}
Images
z
y
x
CASE (ii)
z
x
α_1
C_{x_1}
z
y
Γ_0
Γ_0
x

FIG. 1-3

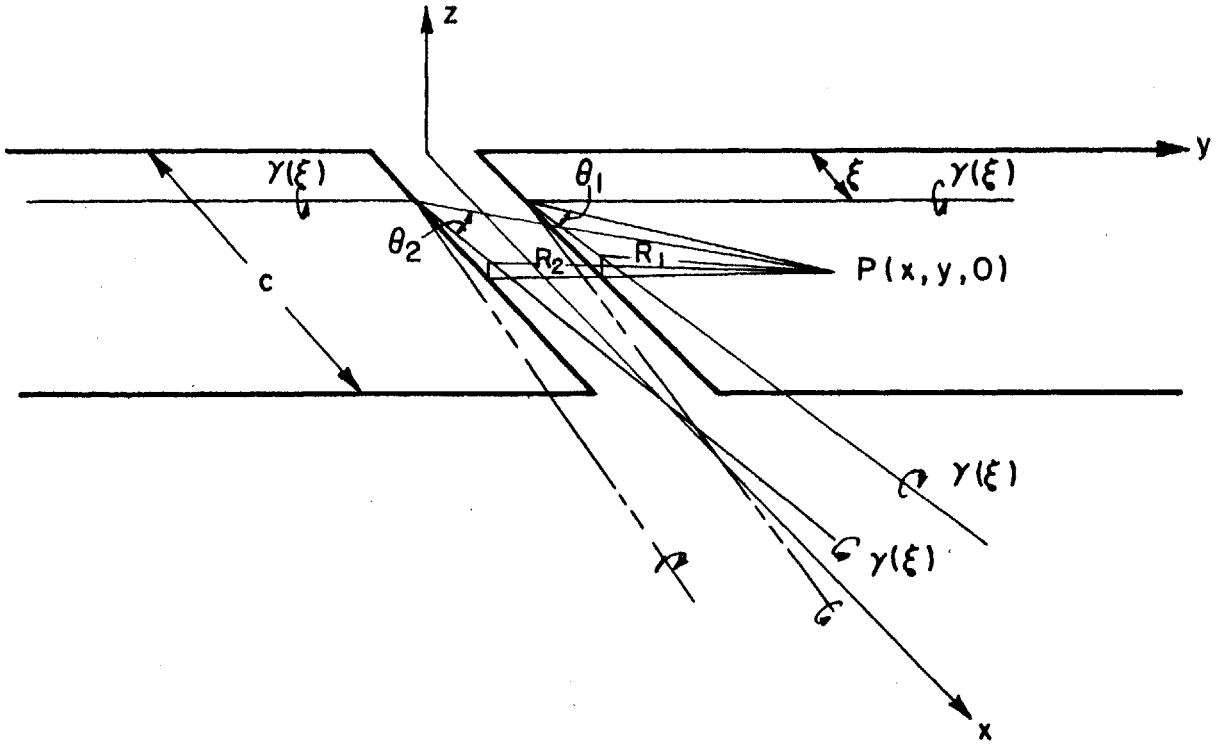

FIG. 1-4 CASE (i)

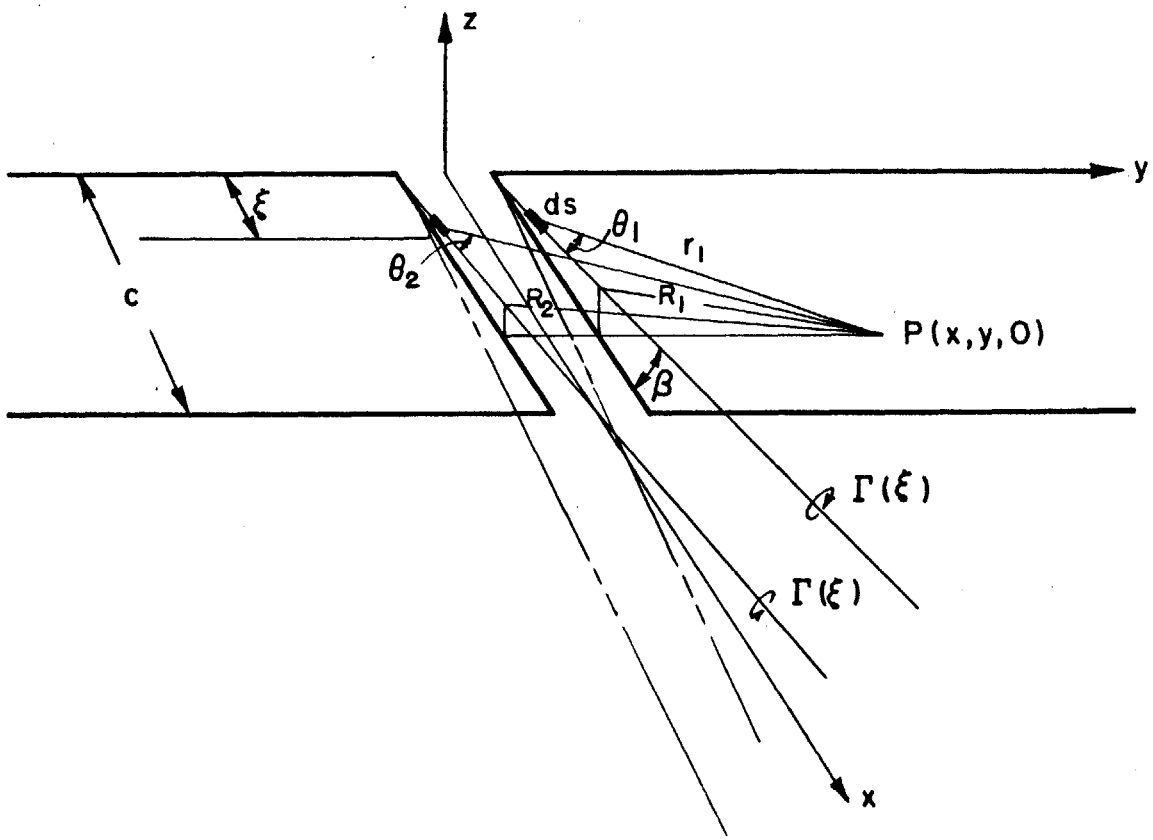

FIG. 1-5 CASE (ii)